Local signal processing in mouse horizontal cell dendrites

Camille A. Chapot[1-3], Luke E. Rogerson[1-4], Tom Baden[1,5], Sinziana Pop[1-3], Philipp Berens[1,2,4], Thomas Euler[1,2,4] *, Timm Schubert[1,2] *

[1]*Institute for Ophthalmic Research, University of Tübingen, 72076 Tübingen, Germany*
[2]*Center for Integrative Neuroscience, University of Tübingen, 72076 Tübingen, Germany*
[3]*Graduate Training Centre of Neuroscience, University of Tübingen, 72076 Tübingen, Germany*
[4]*Bernstein Center for Computational Neuroscience, University of Tübingen, 72076 Tübingen, Germany*
[5]*School of Life Sciences, University of Sussex, Brighton, United Kingdom*
**corresponding authors*

thomas.euler@cin.uni-tuebingen.de
timm.schubert@cin.uni-tuebingen.de

Abstract

The mouse retina contains a single type of horizontal cell, a GABAergic interneuron that samples from all cone photoreceptors within reach and modulates their glutamatergic output via parallel feedback mechanisms. Because horizontal cells form an electrically-coupled network, they have been implicated in global signal processing, such as large scale contrast enhancement. Recently, it has been proposed that horizontal cells can also act locally at the level of individual cone photoreceptor axon terminals. To test this possibility physiologically, we used two-photon microscopy to record light-evoked Ca^{2+} signals in cone axon terminals and horizontal cell dendrites as well as glutamate release in the outer plexiform layer. By selectively stimulating the two mouse cone opsins with green and UV light, we assessed whether signals from individual cones remain "isolated" within horizontal cell dendritic tips, or whether they spread across the dendritic arbour. Consistent with the mouse's opsin expression gradient, we found that light responses recorded from dendrites of dorsal horizontal cells were dominated by M- and those of ventral horizontal cells by S-opsin activation. Light responses measured in neighbouring horizontal cell dendritic tips varied markedly in their chromatic preference, arguing against global processing. Rather, our data support the idea that horizontal cells can process cone input locally, extending the "classical" view of horizontal cells function. Pharmacologically removing horizontal cells from the circuitry reduced the sensitivity of the cone signal to low frequencies, suggesting that local horizontal cell feedback shapes the temporal properties of cone output.

Abbreviations

Ci, consistency index; cone, cone photoreceptor; Cx57, connexin57; d_{base}, distance to the cone axon terminal base; DLi, dark light index; GUW, green UV white stimulus; HC, horizontal cell; NBQX, 6,7-dinitroquinoxaline-2,3-dione; OPL, outer plexiform layer; P*, photoisomerization; Qi, quality index; rod, rod photoreceptor; ROI, region of interest; SC, spectral contrast; SR101, sulforhodamine 101; VGCC, voltage gated calcium channel.

Introduction

Most neurons in the brain have elaborate dendritic arbours that are capable of much more than simply integrating synaptic input. Studies of neurons from different brain regions, such as cerebellar Purkinje cells [1], cortical pyramidal cells [2,3], hippocampal neurons [4] and retinal amacrine cells [5,6], have demonstrated that dendrites can be functionally highly compartmentalized. In some cases, multiple dendritic units can both process synaptic input and generate synaptic output independently and at a local scale (reviewed by [7]). The cellular mechanisms supporting local dendritic processing include anatomical specialisations, differential distribution of active channels, and the local restriction of intracellular signalling (reviewed in [8]). Moreover, computational work suggests that dendrites can even switch between local and global signal processing, depending on the stimulus strength [9]. Such (dynamic) functional compartmentalisation of dendritic arbours greatly increases the computational power of single neurons and, therefore, that of the whole brain.

So far, dendritic processing in the retina has been mainly studied in ganglion cells [10–12] and amacrine cells [5,6]. Here, dendritic subunits vary dramatically in size and function: For example, starburst amacrine cell dendritic arbours are divided in larger sections that individually compute direction of visual motion [13–15], while individual dendritic varicosities of A17 amacrine cells provide local reciprocal feedback to individual rod bipolar cell terminals, at least under low-light conditions [5]. However, also the outer retinal circuitry contains a candidate for dendritic processing, the horizontal cell (HC). This is a GABAergic interneuron that provides reciprocal feedback to photoreceptors and shapes their transmitter release [16–19].

In most vertebrates, HCs come in two types, with one of them bearing an axon with an extended axon terminal system [20]. In the mouse, there is only a single type of (axon-bearing) HC [20,21]. Horizontal cell dendrites contact the axon terminals of cone photoreceptors (cones), while their axon terminal system contacts those of rod photoreceptors (rods). Despite this separation, cone signals travel from the HC's soma to its axon terminal system but whether rod signals can travel from the axon terminal system to the dendrites is controversial [22,23]. Traditionally, HCs have been implicated in global processing, such as contrast enhancement and the generation of antagonistic centre-surround receptive fields (reviewed by [24]). This is consistent with the fact that HCs form a gap junction-coupled network [25], which allows averaging signals across many cones. However, recent studies suggest that HCs support also a local "mode of operation" and that HC feedback can act at the level of a single synaptic contact between a HC dendritic tip and a cone ([19,26]; for discussion see [27]) (Fig. 1A,B).

Here, we test this idea by recording light stimulus-evoked signals at the HC-cone synapse in a slice preparation of the mouse retina using two-photon Ca^{2+} [28,29] and glutamate imaging [30]. We exploited the particular retinal distribution of mouse cone types to discriminate between the global and local processing hypothesis: Mice express two types of cone opsins, a short (S, "UV") and a medium (M, "green") wavelength-sensitive opsin. So-called "true" S-cones [31] exclusively express S-opsin and are homogenously distributed across the retina, while M-cones co-express both opsins at a ratio that changes from M- to S-opsin-dominant along the dorso-ventral axis [32]. Thus, recording at different retinal locations with stimuli of different wavelengths makes it possible to test to what extent the signals of neighbouring cones "mix" in the postsynaptic HC dendritic process. We found that cone signals indeed remain local in the

85 contacting HC dendritic tips, suggesting that HCs support a local mode of operation and
86 dendritic processing. In addition, we show how this local feedback may contribute to temporal
87 shaping of cone output.

Results

Identification of cone axon terminals and horizontal cell processes in the mouse retinal slice

We recorded Ca^{2+} signals in retinal slices prepared from transgenic mice ($Cx57^{+/cre}$ x Ai38; see also Discussion), which express the Ca^{2+} biosensor GCaMP3 in HCs under the control of the promoter for the gap junction-forming connexin57 (Cx57). Based on their GCaMP3 expression, HC processes could be identified in the outer plexiform layer (OPL) in retinal slices (Fig. 1C). To identify cone axon terminals, we bath-applied SR101 [33], which labels synaptically active photoreceptor axon terminals due to uptake of SR101 from the extracellular solution during vesicle endocytosis [34]. We confirmed that the (larger) SR101-labelled structures in the OPL were cone axon terminals by evaluating the method on slices prepared from the HR2.1:TN-XL mouse line [29], in which exclusively cones express TN-XL (Fig. 1D).

Figure 1. Identification of cone axon terminals and HC processes in mouse retinal slices

Light-evoked Ca^{2+} signals in horizontal cell processes

To record light-evoked signals in HC dendrites, we imaged fields in the OPL while presenting green, UV or "white" light flashes ("GUW protocol", Methods) (Fig. 1E,F). In each field, we defined "anatomical" regions-of-interest (ROIs) using the time-averaged GCaMP3 fluorescence image (Methods) to read-out local Ca^{2+} signals in HC dendritic segments. We considered only ROIs that responded to white flashes and fulfilled two strict quality criteria, a quality index (*Qi*) and a consistency index (*Ci*) (Suppl. Fig. 1; Methods), yielding 423 ROIs (4.3% from a total of

9,912 anatomically defined ROIs) with reliable light responses for further analysis (Suppl. Fig. 1A-C).

Because the structural layout of the cone synapse is highly stereotypical [35], we assumed that ROIs located close to the cone axon terminal base are likely to be HC dendritic tips, since this is where these tips make invaginating contacts with the cones (reviewed by [27]). ROIs well above the cone base are expected to belong mostly to HC axon terminal tips (contacting rods), whereas ROIs below the cone base should be located on HC primary dendrites [36]. To get an estimate of each ROI's identity, we manually determined the base of the cone terminals as a "landmark" (solid lines in Fig. 1A,C-E) in each imaged field based on the SR101 labelling and estimated the distance (d_{base}) to the cone axon terminal base for each ROI. Responsive ROIs were most frequent just above the cone axon terminal base (61.5% ROIs within $0 < d_{base} < 5$ µm), within the OPL band occupied by cone terminals. Here, ROIs had the highest *Qi* values (Suppl. Fig. 1D) and the largest light-evoked Ca^{2+} signals (Suppl. Fig. 1E), suggesting that we can indeed locally measure responses from HC dendritic processes in or very close to the cone synapse.

Mechanisms underlying light-evoked Ca^{2+} responses in HCs

To confirm that the Ca^{2+} responses were mediated by glutamate release from photoreceptors, we puff-applied the AMPA/KA-type glutamate receptor antagonist NBQX (200 µM) while presenting light flashes (Fig. 2A,B). NBQX significantly decreased the Ca^{2+} baseline level (F_0) in HC processes (by -1.47 ± 0.07 s.d., mean ± SEM, $p=2.384 \cdot 10^{-7}$, Wilcoxon signed-rank test; n=23 ROIs from 4 slices, 2 mice) and virtually abolished light-evoked Ca^{2+} signals, as indicated by a significant reduction in response amplitude (ΔF; control, 1.24 ± 0.16; NBQX, 0.16 ± 0.03;

128 p=2.384·10^{-7}) and area-under-the-curve (F_{Area}; control, 1.02 ± 0.17; NBQX, -0.01 ± 0.04;
129 p=4.768·10^{-7}) for white flash stimuli (Fig. 2C-E, Table 1).

130 ***Figure 2. Light-evoked Ca^{2+} responses in HC processes are mediated by activation of***
131 ***AMPA/kainate-type glutamate receptors***

132 ***Table 1. Pharmacology for AMPA/KA-type glutamate receptors***

133 Earlier experiments on isolated mouse HCs showed that intracellular Ca^{2+} is modulated by influx
134 through Ca^{2+} permeable AMPA/KA receptors, L-type voltage-gated Ca^{2+} channels (VGCCs) and by
135 release from internal Ca^{2+} stores [37]. To test how these pathways contribute we evoked Ca^{2+}
136 signals in HC dendrites we puff-applied a mixture of AMPA (50 µM) and KA (25 µM) before and
137 in the presence of blockers (Suppl. Fig. 2; Table 2). The response amplitudes (ΔF) to AMPA/KA
138 puffs alone decreased during the experiment (Suppl. Fig. 2A), possibly caused by
139 downregulation of VGCCs and/or Ca^{2+} stores due to the strong pharmacological stimulus. We
140 estimated this run-down from two consecutive control puffs by calculating the ratio of the
141 response amplitudes ($\Delta F_2/\Delta F_1$). When applying the L-type VGCC blocker verapamil (100 µM)
142 during the second AMPA/KA puff, we found $\Delta F_2/\Delta F_1$ to be significantly reduced compared to
143 control (control: $\Delta F_2/\Delta F_1$=0.56 ± 0.06, n=23 ROIs from 2 slices, 2 mice; verapamil:
144 $\Delta F_2/\Delta F_1$=0.23 ± 0.05, n=18/3/2, p=9.088·10^{-5}, Wilcoxon signed-rank test) (Suppl. Fig. 2B,D,E),
145 confirming that these channels contributed to the signals. Similarly, we tested if intracellular
146 Ca^{2+} stores could be involved in amplifying Ca^{2+} signals in HC processes. We bath-applied the
147 sarco-endoplasmic reticulum Ca^{2+} ATPase (SERCA) inhibitor thapsigargin (5 µM), which blocks
148 Ca^{2+} store refill and leads to depletion of Ca^{2+} stores [38]. Thapsigargin decreased the response

ratio, albeit not significantly, given correction for multiple comparisons (thapsigargin: $\Delta F_2/\Delta F_1$=0.34 ± 0.08, n=13 ROIs from 5 slices, 3 animals, p=0.049) (Suppl. Fig. 2C-E). Thus, release from stores may contribute to Ca^{2+} signals in HC dendrites.

Table 2. Pharmacology to block voltage-gated Ca^{2+} channels and Ca^{2+} release from stores

Horizontal cells modulate their own activity via GABA release and subsequent activation of $GABA_A$ auto-receptors [17,19]. Therefore, we tested pharmacologically if GABA auto-reception affects light-evoked Ca^{2+} signals in HC processes. Activation of $GABA_A$ receptors significantly increased Ca^{2+} baseline levels but did not change response size (for details, see Suppl. Material, Suppl. Fig. 3 and Suppl. Table 1), consistent with results for mouse cone axon terminals (for discussion, see [16]).

In summary, the observed light-evoked Ca^{2+} signals in HC processes result from a combination of Ca^{2+} sources, including Ca^{2+}-permeable glutamate receptors, VGCCs and likely Ca^{2+} stores, and are modulated by GABA auto-reception, in agreement with earlier findings [17,37,39–41].

Light-evoked Ca^{2+} signals in HCs reflect the dorsal-ventral opsin expression gradient

Next we recorded HC light responses at different locations along the dorso-ventral axis of the retina, using the mouse' opsin expression gradient as a "tool" to specifically activate different combinations of S- and M-cones (potentially together with rods) with our GUW stimulus. The mouse retina contains mainly M-cones and only 5% "true" S-cones [31]. However, in the ventral retina, ontogenetic M-cones co-express large amounts of S-opsin and, thus, are "functional S-cones" [32,42,43]. Therefore, if the spectral preference of the HC responses reflects this

gradient, this indicates that cones (and not rods) dominantly drive the measured HC signals, consistent with the idea that we are recording from HC dendrites.

To address this question, we determined the spectral contrast (*SC*, Methods) of each ROI as a function of its location along the dorso-ventral axis (Fig. 3). In accordance with the reported cone opsin gradient [43], we found that dorsal HC responses were dominated by M- and ventral HC responses by S-opsin activation (Fig. 3A,B). ROIs located close to the cone axon terminal base ($-4 \leq d_{base} \leq 4$ µm) had significantly higher absolute SC values ($|SC_{-4...+4}|=0.717 \pm 0.022$, n=342) than ROIs below ($d_{base} < -4$ µm, $|SC_{<-4}|=0.417 \pm 0.045$, n=28, $p=1.611 \cdot 10^{-5}$, Wilcoxon rank-sum test) (Fig. 3C). This suggests that the distal tips reflect the contacted cone's chromatic preference and, thus, local signals. More proximal dendrites, on the other hand, average across cones, and thus, show spatial integration, in agreement with the "funnel" shape of the d_{base} vs. *SC* plot (Fig. 3A,B; see next section). In the transitional zone in the central retina, both a UV- and a green-dominated ROI population co-existed (Fig. 3D). Opsin immunostaining of recorded slices from the central retina confirmed that this distribution of UV and green ROIs along the naso-temporal axis reflects cone opsin expression (Fig. 3E): In the nasal part of the slice ROIs were UV-sensitive, whereas in the temporal part of the slice we found green-sensitive ROIs, consistent with the transitional zone not running parallel to the naso-temporal axis but slanted (Fig. 3E, right scheme) [42,43]. Together, our data indicate that the activity recorded in ROIs close to the cone axon terminal base is mostly cone-driven and likely reflects activity in HC dendritic tips.

Figure 3. Light-evoked Ca^{2+} signals in HC dendrites reflect the dorso-ventral cone opsin expression gradient and local cone input

Light-evoked Ca^{2+} signals in HC dendritic tips reflect local activity

Next we assessed if signals from individual cones remain "isolated" within HC distal dendrites or if they spread across the cells' dendritic arbours (or the electrically coupled HC network) (Fig. 1B). We looked for recording fields where neighbouring ROIs have different *SC* preferences (i.e. contain ROIs with $SC > 0$ and ROIs with $SC < 0$). Indeed, this was the case for 15 out of a total of 125 recording fields in both dorsal (5 fields; Fig. 3F) and ventral retina (10 fields; Fig 3G).

To quantify this finding, we focused on "purely" UV and green ROIs ($|SC| > 0.3$; 7 fields, 43 ROIs) and analysed the distribution of the lateral distance between each UV ROI and its neighbours (Fig. 3H). We found that UV ROIs clustered in close proximity (< 10 µm) of each UV ROI – suggesting that they are driven by the same cone axon terminal –, while the majority of green ROIs clustered at larger distances (> 10 µm). The distribution of green ROIs appeared to be periodic with the average distance approximating that between cone axon terminals (approx. 8 µm, *cf*. Fig. 1C,D), indicating that these (green) ROIs were likely driven by other cones. This suggests that ROIs close to the cone axon terminal base represent distal dendritic tips with local cone input.

HC dendritic processes "inherit" properties of the presynaptic cone

If HC dendritic tips reflect the local cone output, the measured signals are expected to share some properties with signals measured in cones. To test this, we presented a coloured noise stimulus (Methods) and measured correlations between neighbouring cone axon terminals (in HR2.1:TN-XL mice, *cf*. Fig. 1D) and between neighbouring HC dendritic tips in the dorsal retina (Fig. 4). If HCs integrated signals globally – e.g. by averaging across a HC's dendritic arbour or by

212 electrical HC coupling –, we would expect a higher correlation between HC dendritic tips for the
213 two stimulus classes, due to the lateral signal spread, than for cone axon terminals.

214 ***Figure 4. In the dorsal retina, light-evoked Ca^{2+} signals in neighbouring cone axon terminals***
215 ***and neighbouring HC dendrites show similar degrees of decorrelation***

216 We calculated the linear correlation coefficient (ρ) between Ca^{2+} traces from cone ROIs (Fig. 4A-
217 C) in the same recording field, in response to coloured noise and, for comparison, to the GUW
218 stimulus (Fig. 4G,H). Because the noise is a weaker stimulus compared to the GUW flashes, the
219 correlation between cone terminal responses significantly decreased for the noise, both when
220 only considering negative transients (GUW: ρ=0.333 ± 0.052, n=26 ROIs (6 fields), 3 slices, 1
221 mouse; noise: ρ=0.098 ± 0.007, n=457 ROIs (65 fields), 7 slices, 3 mice; $p=3.888 \cdot 10^{-5}$, Wilcoxon
222 rank-sum test; Fig. 4G) and when comparing whole traces (GUW: ρ=0.430 ± 0.067; noise:
223 ρ=0.244 ± 0.008; p=0.007; Fig. 4H). We then repeated this experiment on HCs in $Cx57^{+/cre}$ x Ai38
224 mice (Fig. 4D-F) and indeed, like for the cones, the correlation between HC responses decreased
225 for coloured noise compared to GUW stimulation, when considering negative transients (GUW:
226 ρ=0.205 ± 0.015, n=262 ROIs (60 fields), 21 slices, 9 mice; noise: ρ=0.056 ± 0.008, n=344 ROIs
227 (57 fields), 21 slices, 7 mice; $p=1.27 \cdot 10^{-17}$; Fig. 4G) and when comparing whole traces (GUW:
228 ρ=0.275 ± 0.017; noise: ρ=0.204 ± 0.013; p=0.0009; Fig. 4H).

229 A direct comparison between the two sets of experiments is complicated by several factors (e.g.
230 different scan rates for GUW vs. noise stimuli, different biosensors in cones vs. HCs, different
231 ROI sizes) that influence the estimation of response correlation. Nevertheless, our finding that
232 noise stimulation results in similar levels of decorrelation of both the pre- (cone) and the

233 postsynaptic (HC) signal argues in favour of highly local, independent signal processing in HC
234 distal dendrites. This is further supported by the finding that HC dendrites receiving input from
235 the same cone show higher degree of correlation (correlation between negative events vs.
236 distance for GUW stimulus: Spearman R=-0.056, critical value=0.076 for noise stimulus:
237 Spearman R=-0.271, critical value=0.058, Spearman rank correlation test; Suppl. Fig. 4).

238 We also used the Ca^{2+} responses to the noise stimulus to estimate the temporal receptive field
239 (time kernels, see Methods; [44]). In cone axon terminals (Fig. 4I) and HC dendritic tips (Fig. 4J),
240 the time kernels computed using negative transients in the Ca^{2+} trace (*cf*. Fig. 4C,F) displayed
241 robust positive deflections, suggesting that the stimulus was driving the cells efficiently and that
242 mainly light-evoked events contributed to the kernels (both cones and HCs respond with a
243 decrease in Ca^{2+} to an increase in light intensity). Grouping cone ROIs by their spectral
244 preference (derived from their time kernels, see Methods) into green, UV, and mixed revealed a
245 fraction of ~4% UV ROIs (Fig. 4I), closely matching the fraction of S-cones in the dorsal mouse
246 retina [31]. The averaged time kernels of the different groups looked similar for cones and HCs
247 (Fig. 4I,J); cone kernels appeared to be slightly faster, likely due to differences in biosensor
248 properties (TN-XL: τ_{decay}=0.2 s, K_D *in vitro*=2.2 µM, from [45]; GCaMP3: τ_{decay}=0.23 s, K_D *in*
249 *vitro*=0.66 µM, from [28,46]). HC kernels were noisier than those of cones. This may be related
250 to differences in ROI area (cones, 9.6 ± 0.2 μm^2, n=457 ROIs; HCs, 1.9 ± 0.1 μm^2, n=344 ROIs)
251 and, thus, different spatial averaging. The fact that we observed UV-selective kernels in HC
252 dendritic tips just as in cones adds further evidence to the notion that HC dendritic tips can
253 process information locally (*cf.* Fig. 3).

We also tested whether the cone contrast preference was inherited in HC dendrites by presenting colour flashes with different contrasts (Methods, protocol (c)). We found that the contrast preference in HC processes varied systematically along the dorso-ventral retina axis (see Suppl. Material, Suppl. Fig. 5), a trend that is reminiscent of what was earlier shown for cones [43].

Local HC feedback may shape temporal properties of cone responses

Finally, we assessed the effect of local HC feedback on the cone response. To this end, we presented a 60 Hz full-field binary noise stimulus to slices prepared from HR2.1:TN-XL mice (Fig. 5A,C) and mice expressing iGluSnFR (Fig. 5B,D) (Methods; [47]). We estimated time kernels of Ca^{2+} signals in cones and glutamate signals in the OPL as described above (*cf*. Fig. 4). The averaged time kernels were more transient for iGluSnFR in comparison to those for Ca^{2+} (Fig. 5E), likely reflecting differences in signal (Ca^{2+} vs. glutamate) and biosensor kinetics ($\tau_{decay} \approx$ 200 ms for TN-XL vs. 92 ms for iGluSnFR, [30]). For further analysis, we computed the periodograms of the time kernels using discrete Fourier transforms [19] and examined the difference in their power spectral density for each frequency components (Methods and Fig. 5F). We first performed two consecutive recordings with an interval of 5 minutes as controls. No significant differences were found between controls for time kernels from both cone Ca^{2+} (n=61 ROIs, 11 slices, 3 mice) and glutamate release (n=76 ROIs, 15 slices, 3 mice). Next, we deprived HCs from their input by bath application of NBQX (100 µM) and assessed the effect on the time kernels and their corresponding periodograms for cone Ca^{2+} (n=48 ROIs, 15 slices, 3 mice) and glutamate release (n=47 ROIs, 18 slices, 3 mice). Although the time kernels looked narrower after NBQX application, no significant differences were found between these kernels with

respect to time-to-peak and F_{Area} [48]. However, the analysis of the periodograms revealed a significant reduction of the power spectral density at low frequencies (cone Ca^{2+}, at 1 Hz, $p=3\cdot10^{-4}$, dependent samples t-test; glutamate release, at 0 Hz, $p=3.2\cdot10^{-7}$, and at 1 Hz, $p=4.7\cdot10^{-5}$), indicating that local HC feedback contributes to temporal shaping of cone output by increasing the sensitivity of the cone signal to low frequency signal components.

Figure 5. Local HC feedback modulates temporal properties of cone response

Discussion

Because of their large dendritic fields and strong gap-junctional coupling, HCs are "traditionally" thought to play a role in global processing and to provide lateral inhibition, e.g. for contrast enhancement, in the outer retina (reviewed in [27]). Recent studies, however, suggest the existence of a local processing mode, in which HCs provide locally "tailored" feedback to individual cones [19,26] – reminiscent of the local dendritic processing that has been shown for amacrine cells in the inner retina (e.g. [5]).

Here, we tested this hypothesis by recording light stimulus-evoked pre- and postsynaptic activity at the cone-HC synapse in the mouse retina: Two lines of evidence support that mouse HCs process cone input in a highly local and independent manner: First, neighbouring dendritic tips – presumably postsynaptic to different cone axon terminals – differed in their chromatic preferences, reflecting the local cone input. The ubiquitous GCaMP3 expression in HCs did not allow us to assign ROIs to individual HCs and therefore, it is possible that two neighbouring ROIs with different spectral preferences belonged to different HCs. However, it is unlikely that our data are solely explained by recording two overlapping "kinds" of HCs with opposite spectral preference, because mouse HCs indiscriminately contact all cones within their dendritic field [39,49]. Second, the correlation levels of Ca^{2+} signals measured in neighbouring HC dendritic tips were similar to those recorded in neighbouring cone axon terminals. If cone inputs were already averaged at the level of the distal HC dendrite, we would have expected an increase in correlation from cones to HCs. Hence, our correlation data supports local processing in HC dendritic tips – that is at the site where HCs provide feedback to cones. By isolating HCs pharmacologically from their cone input, we then showed that (local) HC feedback may shape

the temporal filtering properties of the cone synapse, i.e. by modulating the power at low stimulus frequencies. We further confirmed that this effect was not only present in the Ca^{2+} signal in the cone axon terminal but also at the level of released glutamate. Taken together, our study extends the "traditional" view of global signalling in HCs by a crucial local component, indicating that dendritic processing already happens at the first synapse of the retina.

Local vs. global HC feedback

The idea that HCs may provide local feedback was first introduced by Jackman and colleagues [26], who showed that focal uncaging of MNI-glutamate in the OPL led to a local increase in cone Ca^{2+}, indicative of local, positive feedback from HCs. They proposed that both local and global feedback are triggered by the activation of AMPA/KA receptors on HCs, but with local feedback being mediated by the local Ca^{2+} in the HC dendrite and global feedback relying on membrane depolarisation and possibly amplification by VGCCs [50]. They suggested that while the two feedback pathways acted in concert at a similar time-scale, their effects would not cancel out due to the difference in spatial scale.

The "mixing" of S- and M-opsin signals in more proximal HC dendrites (Fig. 3C) hints at some degree of signal integration and potentially global processing also in mouse HCs; however, we did not find interactions between distal HC dendrites, the sites where the feedback to cones is generated. While we cannot exclude that our experimental conditions (slices) favoured local processing, we think that this is unlikely for the following reasons: First, lateral inhibition has been demonstrated in cones recorded in retinal slices (≥300 µm thick) under similar experimental conditions [16]. Second, patch clamp recordings of AII amacrine cells in mouse

retinal slices showed that gap junctional coupling is intact, supporting that electrical coupled networks are functional in this preparation [51,52]. Third, earlier work suggests that local (positive) feedback is more sensitive to the preparation (slice vs. wholemount) than global feedback [26].

Global feedback requires integration of signals within one HC, or within the HC network via gap-junction coupling with Cx57 [25]. In the present study, one *Cx57* allele is deleted and replaced by a *cre* gene in the $Cx57^{+/cre}$ x Ai38 mouse line. The deletion of one allele results in a reduced expression of Cx57, which leads to a decrease in HC receptive field size by a third and an elevated resting membrane potential [53]. However, in the same mouse line, injections of a gap junction-permeable tracer into individual HCs revealed coupled networks of 100 HCs on average. Moreover, even fully deleting Cx57 did not change dendritic arbour size [53]. Thus, since strong HC coupling is still present and synaptic connections between HCs and photoreceptors seem unaltered [53], we do not expect this genetic modification to substantially affect our experimental results.

Mechanism of local Ca^{2+} signalling in HC dendrites

What is the cellular basis of the local Ca^{2+} signalling we observed in HC dendrites? In line with previous studies of mouse HCs [37,39,41], we show that these signals are mediated by a combination of Ca^{2+} permeable AMPA/KA-type glutamate receptors, VGCCs and possibly Ca^{2+} released from stores. This combination is reminiscent of another reciprocal synapse, for which local signal processing was demonstrated: the synapse between rod bipolar cells (RBCs) and A17 amacrine cells in the inner retina [54]. Here, Ca^{2+} enters a dendritic varicosity via AMPA

receptors and triggers GABA release, with the necessary amplification of the Ca^{2+} signal generated by Ca^{2+}-induced Ca^{2+} release from stores. To keep the signal from spreading to neighbouring varicosities, A17 cells express Ca^{2+}-activated potassium (BK) channels that hyperpolarize the varicosity and thereby suppress activation of VGCCs. In addition, varicosities are spaced with a minimal distance of ~20 µm along the dendrite to increase electrical isolation. This arrangement also allows – in principle – switching to a more global processing mode, since stronger stimulation may overcome the BK channel-mediated suppression of VGCC activation and foster spreading of electrical signals along the A17 dendrites [5,54]. It is conceivable that the local signalling in HCs employs a similar mechanism: (*i*) As shown for zebrafish, tiger salamander, anole lizard and rabbit HCs by Jackman et al. [26], local HC feedback can be triggered by AMPA receptor activation without requiring VGCCs. If this is also true for feedback in mouse HC, however, is still unclear; while we found AMPA/KA puff-evoked Ca^{2+} responses to involve L-type VGCCs, this may be different for light-evoked Ca^{2+} signals, which likely reflect more physiological conditions. In fact, activity of VGCCs in HCs is suppressed by dopamine, which is released in a light-dependent fashion [55], suggesting that under our light levels VGCCs may contribute less to the Ca^{2+} signal. (*ii*) HCs express BK channels that limit membrane depolarisation in a voltage- and Ca^{2+}-dependent manner [56]. (*iii*) Ca^{2+} signals in HC dendrites partially rely on Ca^{2+} stores [37]. (*iv*) The HC morphology may support electrical isolation between dendritic tips (discussed in [27]; C. Behrens, personal communication).

An important difference to the RBC-A17 synapse (and another level of complexity) is that an HC affects its own activity not only by modulating the output of its presynaptic partner (the cone),

but also by sensing its GABA release via $GABA_A$ auto-receptors [16,40]. A17 cells also express $GABA_A$ receptors but they are not thought to be involved in auto-reception [57].

Do rods contribute to the Ca^{2+} signals in HC dendrites?

The transgenic mouse line used here expresses GCaMP3 in all HC compartments and because dendritic and axonal HC processes are intermingled in the OPL, we could not distinguish them purely based on their morphological appearance. Yet, our conclusions rely on the assumption that the Ca^{2+} signals we measured reflected cone-mediated input and that rod input could be neglected. We think that this was the case for two reasons: (*i*) The largest Ca^{2+} signals we measured were located at the OPL level where HC dendrites enter invaginations in the cone axon terminal base (e.g. [27,58]). (*ii*) The chromatic tuning of these Ca^{2+} signals depended on the slice position along the retina's dorso-ventral axis and reflected the local ratio of S- vs. M-opsin expression – dorsal and ventral HC responses were strongly dominated by UV and green responses, respectively. If rods had responded substantially to either UV or green stimuli, we would have expected an additional UV response in dorsal HCs and/or an additional green response in ventral HCs.

Why we did not detect any rod responses is unclear; as we recently showed that RBCs respond to light-on stimuli under similar experimental conditions [47]. One possible explanation is that rods were saturated and the RBCs were driven by cones, because in mice, ~70% of the RBCs contact at least one cone [59] and therefore may receive substantial cone input.

Functional consequences of local Ca^{2+} signalling for HC feedback to cones

Local HC processing is expected to affect chromatic processing: In some mammals, including macaques and rabbits, feedback from axon-less HCs is thought to provide cones with a colour-opponent receptive field surround [60,61], which requires these HCs to average across cones and, thus, perform some degree of global processing. Mice lack an axon-less HC type [21]. If the dominant form of feedback in axon-bearing HCs was indeed local, as suggested by our data, it would argue against a prominent role for HCs in chromatic processing in mice (see discussion in [27]. This is in line with the lack of colour-antagonistic responses in mouse bipolar cells at the level of somatic voltage [62].

What could be the purpose of local HC feedback to cones? Our pharmacological data hints that – within the limits of our stimulus (60 Hz binary noise) –, HC feedback may shape the transmission of low frequency signals in the cone output. Under our experimental conditions, local signalling appeared to be the main processing mode in mouse HCs, therefore increasing the bandwidth in the low-frequency range may be a specific function of local HC feedback.

In theory, the objective of sensory neurons is often considered to be the transmission of the maximum information content from a sensory input, given a limited metabolic capacity [63]. Adaptational mechanisms allow the circuitry to robustly meet this objective despite changing natural scene statistics [64–66], whether by enhancing features (thereby increasing information content) or removing redundancy (thereby reducing metabolic cost). For HCs, these elements have typically been considered for adaptation to spatial properties, through mechanisms such as the centre-surround receptive field and background-luminance subtraction. Here, the local adaptation observed appears to operate in the time domain; the effect is made visible by changes in sensitivity to low frequency signal components, which might convey little

information content in natural scenes where they are strongly present, and more information otherwise. In this sense, local feedback may serve temporal contrast enhancement. That the feedback can occur at the level of a single photoreceptor is perhaps not surprising, as such a cell driven in isolation is still subject to trade-offs in information and metabolic cost. In natural scenes, spatial and temporal statistics are not independent, and the interplay between their respective adaptational mechanisms – such as here the potential interplay between local and global feedback mechanisms in HCs – is an attractive subject for further study (see discussion in [27]). A promising approach to tackle these questions may be a combination of voltage biosensors [67,68] to probe the voltage "distribution" across an HC's dendritic arbour with biophysically realistic models.

Materials and Methods

Animals

For the Ca^{2+} imaging experiments in retinal horizontal cells (HCs), we crossed the transgenic mouse lines $Cx57^{cre/cre}$ [41] and B6;129S-*Gt(ROSA)26Sor*$^{tm38(CAG-GCaMP3)Hze}$/J (Ai38) [28], yielding $Cx57^{+/cre}$ x Ai38 mice, which express the Ca^{2+} biosensor GCaMP3 [46] selectively in HCs. For Ca^{2+} imaging in cone axon terminals, we used the HR2.1:TN-XL mouse line [29], which expresses the ratiometric Ca^{2+} biosensor TN-XL [69] exclusively in cones. For glutamate imaging, iGluSnFR [30] was virally expressed after intra-vitreal virus injection in C57BL/6 mice (see Virus injection). Both male and female adult mice (4-18 weeks of age) were used. Animals were deeply anesthetized with isoflurane (CP-Pharma, Germany) and killed by cervical dislocation. All procedures were performed in accordance with the law on animal protection (Tierschutzgesetz) issued by the German Federal Government and approved by the institutional committee on animal experimentation of the University of Tübingen.

Retinal tissue preparation

For all imaging experiments, mice were dark adapted for at least 2 hours and then killed. Under dim red light, both eyes were marked at the ventral side to maintain retinal orientation, quickly enucleated and hemisected in carboxygenated (95% O_2 / 5% CO_2) extracellular solution with (in mM): 125 NaCl, 2.5 KCl, 1 $MgCl_2$, 1.25 NaHCO3, 20 glucose, 2 $CaCl_2$, 0.5 L-glutamine and 150 µM pyridoxal 5-phosphate (a cofactor of the glutamic acid decarboxylase, [70]) (Sigma-Aldrich or Merck, Germany). Cornea, lens and vitreous body were carefully removed. The retina was separated from the eye-cup, cut in half, flattened and mounted photoreceptor side-up on a

nitrocellulose membrane (0.8 µm pore size, Millipore, Ireland). Using a custom-made slicer [71], acute vertical slices (300 µm thick) were cut parallel to the naso-temporal axis. Slices attached to filter paper were transferred on individual glass coverslips, fixed using high vacuum grease and kept in a storing chamber at room temperature for later use. For all imaging experiments, individual retinal slices were transferred to the recording chamber, where they were continuously perfused with warmed (~36°C), carboxygenated extracellular solution containing 0.5 µM sulforhodamine 101 (SR101; Sigma-Aldrich, Germany) to visualize cone axon terminals.

Virus injection

Before the injection of AAV9.hSyn.iGluSnFR.WPRE.SV40 (Penn Vector Core, PA, USA), mice (5-7 weeks) were anaesthetized with 10% ketamine (Bela-Pharm GmbH, Germany) and 2% xylazine (Rompun, Bayer Vital GmbH, Germany) in 0.9% NaCl (Fresenius, Germany). A Hamilton syringe (syringe: 7634-01, needle: 207434, point style 3, length 51 mm, Hamilton Messtechnik GmbH) containing the virus was fixed on a micromanipulator (M3301, World Precision Instruments, Germany) at an angle of 15°. Then, 1 µl of the virus was injected into the naso-ventral part of the vitreous body [47]. Recordings were performed 3 weeks after the injection.

Two-photon imaging

Ca^{2+} and glutamate signals were recorded on a customized MOM-type two-photon microscope (Sutter Instruments, Novato, CA; designed by W. Denk, MPI for Neurobiology, Martinsried, Germany) [33,72], equipped with a mode-locked Ti:Sapphire laser (MaiTai-HP DeepSee; Newport Spectra-Physics, Germany) tuned to either 860 or 927 nm for TN-XL and GCaMP3/iGluSnFR excitation, respectively. Two PMTs with appropriate band-pass filters were

used to detect the fluorescence emission of (a) TN-XL/citrine, GCaMP3 (538 BP 50, AHF, Germany) or iGluSnFR (510 BP 84), and (b) TN-XL/eCFP (483 BP 32) or SR101 (630 BP 60). A 20x water-immersion objective (either XLUMPlanFL, 0.95 NA, Olympus, Germany, or W Plan-Apochromat 20x/1.0 DIC M27, Zeiss, Germany) was employed to acquire time-lapsed image sequences (image series) with the custom software ScanM (by M. Müller, MPI for Neurobiology, and T. Euler) running under IgorPro 6.37 (Wavemetrics, Lake Oswego, OR, USA). Images of 128 x 64 pixels (51.8 x 28.2 µm or 38.7 x 20.8 µm) at a frame rate of 7.8125 Hz were recorded for all visual stimuli except the "coloured noise" and binary noise stimuli (see below), where we used images of 128 x 16 pixels (51.8 x 7.1 µm or 38.7 x 5.2 µm, at 31.25 Hz). Recording fields were always located at the outer plexiform layer (OPL) to prevent bleaching of the cone outer segments by the scanning laser [29,43].

Light stimulation

Full-field light stimuli were generated by two band-pass-filtered LEDs (UV, 360 BP 12; green, 578 BP 10; AHF) driven by an open-source microprocessor board (http://www.arduino.cc) and synchronized with the scanner retrace to avoid light stimulus artefacts during image acquisition. The light from the two LEDs was combined by a beam-splitter (400 CDLP, AHF) and focused on the retinal slice through the bottom of the recording chamber via a condenser lens (H DIC, 0.8 NA, Zeiss). The intensity of each LED was adjusted such that the photoisomerisation (P*) rate in S-cones elicited by the UV LED was equal to the P* rate elicited by the green LED in M-cones [62,73]. The light intensity generated by each LED ranged from $5 \cdot 10^2$ (I_{MIN}) to $6.5 \cdot 10^3$ (I_{MAX}) P*s^{-1}/cone for all stimuli except binary noise stimulus (described below, here $I_{MIN}=6 \cdot 10^2$, $I_{MAX}=19 \cdot 10^3$ P*s^{-1}/cone). Note that we use the term "white" to refer to the simultaneous stimulation with

both LEDs with the same P* rate. An additional background illumination (I_{BKG}) of approx. 10^4 P*s^{-1}/cone was always present due to the scanning two-photon excitation laser [29,43]. All following 5 stimulus protocols were preceded by a 15-s period that allowed the photoreceptors adapting to the background (I_{MIN} + I_{BKG}):

(a) A white flash protocol consisting of 1-s bright flashes (from a background of I_{MIN} to I_{MAX}) of "mouse-white" (both LEDs on) at 0.2 Hz. This protocol was used to assess drug effects on light-evoked Ca^{2+} responses.

(b) A colour flash protocol consisting of bright green, UV and white 1-s flashes ("GUW") at 0.2 Hz and repeated 10 times for each colour (same intensity levels as for (a)). This protocol was used to determine the spectral contrast (*SC*, see below) preference.

(c) A contrast and colour flash protocol consisting of 1-s bright and dark flashes, with the respective LED combinations (green, UV, and white) at I_{MAX} or I_{MIN}, respectively, at 0.2 Hz and repeated 8 times for each condition (Intensity between flashes: $3 \cdot 10^3$ P*s^{-1}/cone). This protocol was used to determine the *SC* and the dark-light index (*DLi*, see below).

(d) A "coloured noise" stimulus protocol consisting of a 25 Hz pseudo-random sequence of green, UV, white, and dark flashes. This protocol was used to probe correlation between neighbouring cones and HC processes and to calculate time kernels (see below).

(e) A binary noise stimulus protocol consisting of a 60-Hz pseudo-random sequence of dark and bright flashes. This protocol was also used to calculate time kernels.

Immunohistochemistry

After two-photon imaging, a subset of retinal slices were fixed with 4% paraformaldehyde (PFA) in 0.1 M phosphate-buffered saline (PBS) at 4°C for 15 min. Slices were then washed in 0.1 M PBS, and submerged in blocking solution (0.1 M PBS, 0.3% Triton X-100, 10% donkey serum) over night at 4°C. Afterwards, slices were incubated for 4 days at 4°C with primary antibodies (rabbit anti-M-opsin (1:1,000) from EMD Millipore, Billerica, MA, USA; goat anti-S-opsin (1:500) from Santa Cruz Biotechnology (Germany) in 0.1 M PBS, 0.3 Triton X-100, and 5% donkey serum. The following day, slices were washed in 0.1 M PBS and incubated with the secondary antibodies (donkey anti-rabbit conjugated to Alexa Fluor 568 (1:1000) and donkey anti-goat conjugated to Alexa Fluor 660 (1:1000), both Invitrogen, Carlsbad, CA, USA). Image stacks (15 frames of 1024 x 1024 pixels, 15 µm Z-steps) were acquired on a confocal laser-scanning microscope (Leica TCS SP8, Germany) which was equipped with green (552 nm) and far-red (638 nm) lasers and a 10x 0.3 NA objective lens (Leica). Maximum-intensity projections of the image stacks were performed using Fiji (http://fiji.sc/Fiji).

Pharmacology and drug application

All drugs were prepared as stock solutions in distilled water or, in the case of thapsigargin, in DMSO, and were stored at -20°C. Before each experiment, drugs were freshly diluted from stock solution in carboxygenated extracellular solution. For puff application, a glass electrode (tip diameter: 1-2 µm) was placed approx. 100 µm above the recorded region of the slice and drug solution was puffed for 10 s using a pressure application system (0.2-1 bar, Sigmann Elektronik GmbH, Germany). The lateral spread of the puff was about 200 µm in diameter, as measured by puffing a fluorescent dye (SR101). For bath application, the tissue was perfused with the drug added to the bathing solution for at least 5 mins (perfusion rate of ~1.5 ml/min). For puff

application, the following concentrations were used (in µM): 200 6,7-dinitroquinoxaline-2,3-dione (NBQX), 50 α-amino-3-hydroxy-5-methyl-4-isoxazolepropionic acid (AMPA), 25 kainic acid (KA), 100 muscimol and 100 SR-95531 hydrobromide (gabazine). For bath application, we used (in µM): 100 verapamil, 5 thapsigargin and 100 NBQX. All drugs were purchased from Tocris Bioscience (Bristol, England) except for KA, which was purchased from Sigma-Aldrich.

Data analysis

To analyse light-evoked Ca^{2+} signals in HCs and cones, as well as glutamate release in the OPL, we used custom-written scripts in IgorPro (Wavemetrics) and SARFIA [74], a freely available package for IgorPro. For GCaMP3 and TN-XL fluorescence (Ca^{2+} in HCs and cones, respectively), regions-of-interest (ROIs) were anatomically defined using SARFIA's automatic Laplace operator feature on the averaged, filtered image series and manually corrected if required (e.g. if two nearby structures shared one ROI); ROIs with an area < 10 pixels were discarded. For iGluSnFR fluorescence (glutamate released from cones), the correlation over time between neighbouring pixels was measured and ROIs were determined based on a correlation threshold (defined for each recording depending on the signal-to-noise (S/N) ratio). ROI diameters were limited to range between 5 to 8 µm (expected diameter of a cone axon terminal). To estimate each ROI's "vertical" position within OPL, the positions of cone axon terminals were visualized using SR101 fluorescence (Fig. 1C,D). A ROI's distance to the cone axon terminal base (d_{base}) was estimated relative to a manually drawn straight line tracing the base of all cone axon terminals in a recorded field.

For TN-XL, the ratio between acceptor (citrine) and donor fluorescence (eCFP) was calculated on the image series, prior to signal extraction. For all indicators, time traces were extracted for each ROI, de-trended by high-pass filtering at ~0.1 Hz (except for the analysis of drug effects on the baseline) and z-normalized (ratio between de-trended trace subtracted from its average and s.d. noise). For all flash stimuli, we determined response amplitude (ΔF), area-under-the-curve (F_{Area}) and, in case of NBQX, muscimol and gabazine puffs, as well as for the contrast and colour flash protocol, also the Ca^{2+} baseline level (F_0). These parameters were measured on the trace smoothed using IgorPro's boxcar algorithm with 2 passes for all stimuli (except for drug experiments, where 5 passes were used).

Two quality criteria were defined to identify responsive ROIs: The **quality index** (*Qi*) is defined as the ratio between ΔF in response to a white flash and the s.d. of the noise of the trace (= raw trace minus the trace smoothed using IgorPro's boxcar algorithm with 2 passes). For stimulus protocol (c), *Qi* was calculated independently for dark and bright flashes. Depending on stimulus and experiment type, we used different *Qi* thresholds applied to the responses to white stimuli (Qi ≥ 1 for all flash protocols except (c) which employed fewer stimulus repeats, where we used *Qi* ≥ 1.5, and for AMPA/KA puffs, where we used Qi ≥ 3). The **consistency index** (*Ci*) is defined as the ratio between the variance of the mean and the mean of the variance across n=8 to 10 stimulus trials [44]. ROIs with *Ci* ≥ 0.2 were considered to show consistent light responses over time. For all experiments involving light stimuli, only ROIs that passed both criteria were included for further analysis.

Depending on the stimulus protocol, we determined additional parameters for each ROI: We calculated the **spectral contrast** preference, $SC = \left(F_{Area(G)} - F_{Area(UV)}\right)/\left(F_{Area(G)} + F_{Area(UV)}\right)$,

using the F_{Area} for the responses to green and UV flashes (protocol (b)). The **dark-light index**, $DLi = \left(F_{Area(B)} - F_{Area(D)}\right)/\left(F_{Area(B)} + F_{Area(D)}\right)$ [43], was determined using the F_{Area} for the responses to bright and dark white flashes (protocol (c)).

The data recorded with the coloured noise stimulus (protocol (d); *cf*. Fig. 4) were analysed by calculating the negative transient-triggered average from the de-trended and z-normalized Ca^{2+} traces, weighted by the transients' amplitudes, yielding a temporal receptive field (time kernel) for each ROI. A ROI was considered light-responsive if the maximum amplitude of the kernel (A_{LRF}) for green and/or UV was $A_{LRF} > 2$ s.d. of the noise. All kernels were then normalized to 1. We then calculated the correlation between ROIs present in the same field either for the full Ca^{2+} traces or for negative events (with amplitudes < -2 s.d. of the noise) in a time window of -750 to 250 ms around the event (at 0 ms). The mean correlation for each field was then used for further analysis. An equivalent approach was used to analyse the data recorded with the binary noise (protocol (e); *cf*. Fig. 5); with ROIs considered responsive if $A_{LRF} > 3$ s.d. noise. A periodogram was generated by applying a discrete Fourier transform (DFT) to the time-series of each kernel without zero padding. The power spectral densities at each frequency component followed approximately a log-normal distribution, and so to improve Gaussianity (assumed in the subsequent t-tests), a log transform was applied to each periodogram, and the transformed data was used for statistical comparisons.

Statistics

All statistical tests (except for the ones for the periodograms) were performed using the Wilcoxon signed-rank test or the Wilcoxon rank-sum test. Alpha was set to 0.05 and p-values (*p*)

588 < 0.05 were considered as significant (*), $p < 0.01$ (**), $p < 0.001$ (***). For multiple
589 comparisons, Bonferroni correction was used and $p < 0.025$ was considered as significant (+),
590 $p < 0.005$ (++), $p < 0.0005$ (+++). For periodograms, a dependent sample t-test was computed for
591 each positive frequency component and Bonferroni correction was used (15 comparisons, *cf.*
592 Fig. 5). Spearman rank correlation test was used to estimate the correlation between negative
593 events and distance along the slice (*cf.* Fig. 4) as well as the relationships between *DLi*, *SC*, slice
594 position and F_0 (*cf.* Suppl. Fig. 5). Differences between dorsal and ventral *DLi* were assessed with
595 t-test and Bartlett test. Errors are given as standard error of the mean (SEM) or standard
596 deviation (s.d.).

597 *Data availability*

598 All data will be available at http://www.retinal-functomics.net upon publication.

Author Contributions

C.A.C., T.S. and T.E. designed the study; C.A.C. and S.P. established the experimental approach; C.A.C. performed experiments and pre-processing; C.A.C. analysed the data, with input from T.S., T.B., L.E.R., P.B., and T.E.; C.A.C., T.S., T.E., and L.E.R., wrote the manuscript, with input from P.B. and T.B.

Acknowledgements

We thank G. Eske for excellent technical assistance and K. Franke for performing the intravitreal virus injection; L.L. Looger, the Janelia Research Campus of the Howard Hughes Medical Institute and the Genetically-Encoded Neuronal Indicator and Effector (GENIE) Project for making the viral construct AAV9.hSyn.iGluSnFR.WPRE.SV40 publicly available.

Funding

This work was supported by the Deutsche Forschungsgemeinschaft (EXC 307, CIN to T.E. and T.S.; SCHU 2243/3-1 to T.S.) and the German Ministry of Science and Education (BMBF) through the Bernstein Award to PB (FKZ: 01GQ1601).

Conflict of Interest Statement

The authors have no conflict of interest.

References

1. Denk W, Sugimori M, Llinás R. Two types of calcium response limited to single spines in cerebellar Purkinje cells. Proc Natl Acad Sci U S A. 1995;92: 8279–8282. doi:10.1073/pnas.92.18.8279

2. Polsky A, Mel BW, Schiller J. Computational subunits in thin dendrites of pyramidal cells. Nat Neurosci. 2004;7: 621–7. doi:10.1038/nn1253

3. Branco T, Clark Beverley A., Häusser M. Dendritic Discrimination of Temporal Input Sequences in Cortical Neurons. Science (80-). 2010;329: 1671–1675.

4. Branco T, Staras K, Darcy KJ, Goda Y. Local Dendritic Activity Sets Release Probability at Hippocampal Synapses. Neuron. 2008;59: 475–485. doi:10.1016/j.neuron.2008.07.006

5. Grimes WN, Zhang J, Graydon CW, Kachar B, Diamond JS. Retinal Parallel Processors: More than 100 Independent Microcircuits Operate within a Single Interneuron. Neuron. Elsevier Ltd; 2010;65: 873–885. doi:10.1016/j.neuron.2010.02.028

6. Euler T, Detwiler PB, Denk W. Directionally selective calcium signals in dendrites of starburst amacrine cells. Nature. 2002;418: 845–852. doi:10.1038/nature00931

7. Branco T, Häusser M. The single dendritic branch as a fundamental functional unit in the nervous system. Curr Opin Neurobiol. 2010;20: 494–502. doi:10.1016/j.conb.2010.07.009

8. Sjöström PJ, Rancz A, Roth A, Häusser M. Dendritic Excitability and Synaptic Plasticity Dendritic Excitability and Synaptic Plasticity. Physiol Rev. 2008;88: 769–840. doi:10.1152/physrev.00016.2007.

9. Remme MWH, Rinzel J. Role of active dendritic conductances in subthreshold input integration. J Comput Neurosci. 2011;31: 13–30. doi:10.1007/s10827-010-0295-7

10. Schachter MJ, Oesch N, Smith RG, Rowland Taylor W. Dendritic spikes amplify the synaptic signal to enhance detection of motion in a simulation of the direction-selective ganglion cell. PLoS Comput Biol. 2010;6: 1–24. doi:10.1371/journal.pcbi.1000899

11. Oesch N, Euler T, Taylor WR. Direction-selective dendritic action potentials in rabbit retina. Neuron. 2005;47: 739–750. doi:10.1016/j.neuron.2005.06.036

12. Sivyer B, Williams SR. Direction selectivity is computed by active dendritic integration in retinal ganglion cells. Nat Neurosci. Nature Publishing Group; 2013;16: 1848–56. doi:10.1038/nn.3565

13. Hausselt SE, Euler T, Detwiler PB, Denk W. A dendrite-autonomous mechanism for direction selectivity in retinal starburst amacrine cells. PLoS Biol. 2007;5: 1474–1493. doi:10.1371/journal.pbio.0050185

14. Ding H, Smith RG, Poleg-Polsky A, Diamond JS, Briggman KL. Species-specific wiring for direction selectivity in the mammalian retina. Nature. Nature Publishing Group; 2016;535: 105–10. doi:10.1038/nature18609

15. Chen Q, Pei Z, Koren D, Wei W. Stimulus-dependent recruitment of lateral inhibition underlies retinal direction selectivity. Elife. 2016;5: 1–19. doi:10.7554/eLife.21053

16. Kemmler R, Schultz K, Dedek K, Euler T, Schubert T. Differential regulation of cone calcium signals by different horizontal cell feedback mechanisms in the mouse retina. J Neurosci. 2014;34: 11826–43. doi:10.1523/JNEUROSCI.0272-14.2014

17. Liu X, Hirano A a, Sun X, Brecha NC, Barnes S. Calcium channels in rat horizontal cells regulate feedback inhibition of photoreceptors through an unconventional GABA- and pH-sensitive mechanism. J Physiol. 2013;591: 3309–24. doi:10.1113/jphysiol.2012.248179

18. Wang T-M, Holzhausen LC, Kramer RH. Imaging an optogenetic pH sensor reveals that protons mediate lateral inhibition in the retina. Nat Neurosci. Nature Publishing Group; 2014;17: 262–8. doi:10.1038/nn.3627

19. Vroman R, Klaassen LJ, Howlett MHC, Cenedese V, Klooster J, Sjoerdsma T, et al. Extracellular ATP Hydrolysis Inhibits Synaptic Transmission by Increasing pH Buffering in the Synaptic Cleft. PLoS Biol. 2014;12. doi:10.1371/journal.pbio.1001864

20. Peichl L, González-Soriano J. Morphological types of horizontal cell in rodent retinae: a

669 comparison of rat, mouse, gerbil, and guinea pig. Vis Neurosci. 1994;11: 501–517.
670 doi:10.1017/S095252380000242X

671 21. Suzuki H, Pinto LH. Response properties of horizontal cells in the isolated retina of wild-
672 type and pearl mutant mice. J Neurosci. 1986;6: 1122–1128.

673 22. Trumpler J, Dedek K, Schubert T, de Sevilla Muller LP, Seeliger M, Humphries P, et al. Rod
674 and Cone Contributions to Horizontal Cell Light Responses in the Mouse Retina. J
675 Neurosci. 2008;28: 6818–6825. doi:10.1523/JNEUROSCI.1564-08.2008

676 23. Szikra T, Trenholm S, Drinnenberg A, Jüttner J, Raics Z, Farrow K, et al. Rods in daylight act
677 as relay cells for cone-driven horizontal cell-mediated surround inhibition. Nat Neurosci.
678 2014;17: 1728–35. doi:10.1038/nn.3852

679 24. Thoreson WB, Mangel SC. Lateral interactions in the outer retina. Prog Retin Eye Res.
680 2012;31: 407–441. doi:10.1016/j.preteyeres.2012.04.003

681 25. Hombach S, Janssen-Bienhold U, Söhl G, Schubert T, Büssow H, Ott T, et al. Functional
682 expression of connexin57 in horizontal cells of the mouse retina. Eur J Neurosci. 2004;19:
683 2633–2640. doi:10.1111/j.1460-9568.2004.03360.x

684 26. Jackman SL, Babai N, Chambers JJ, Thoreson WB, Kramer RH. A positive feedback synapse
685 from retinal horizontal cells to cone photoreceptors. PLoS Biol. 2011;9: 1001058.
686 doi:10.1371/journal.pbio.1001057

687 27. Chapot CA, Euler T, Schubert T. How do horizontal cells “talk” to cone photoreceptors?
688 Different levels of complexity at the cone-horizontal cell synapse. J Physiol. 2017;
689 doi:10.1113/JP274177

690 28. Zariwala HA, Borghuis BG, Hoogland TM, Madisen L, Tian L, De Zeeuw CI, et al. A Cre-
691 Dependent GCaMP3 Reporter Mouse for Neuronal Imaging In Vivo. J Neurosci. 2012;32:
692 3131–3141. doi:10.1523/JNEUROSCI.4469-11.2012

693 29. Wei T, Schubert T, Paquet-Durand F, Tanimoto N, Chang L, Koeppen K, et al. Light-Driven
694 Calcium Signals in Mouse Cone Photoreceptors. J Neurosci. 2012;32: 6981–6994.

doi:10.1523/JNEUROSCI.6432-11.2012

30. Marvin JS, Borghuis BG, Tian L, Cichon J, Harnett MT, Akerboom J, et al. An optimized fluorescent probe for visualizing glutamate neurotransmission. Nat Methods. 2013;10: 162–170. doi:10.1038/nmeth.2333

31. Haverkamp S, Wässle H, Duebel J, Kunner T, Augustine GJJ, Feng G, et al. The primordial, blue-cone color system of the mouse retina. J Neurosci. 2005;25: 5438–5445. doi:10.1523/JNEUROSCI.1117-05.2005

32. Szél A, Röhlich P, Caffé AR, Juliusson B, Aguirre G, Van Veen T. Unique topographic separation of two spectral classes of cones in the mouse retina. J Comp Neurol. 1992;325: 327–342. doi:10.1002/cne.903250302

33. Euler T, Hausselt SE, Margolis DJ, Breuninger T, Castell X, Detwiler PB, et al. Eyecup scope—optical recordings of light stimulus-evoked fluorescence signals in the retina. Eur J Physiol. 2009;457: 1393–1414. doi:10.1007/s00424-008-0603-5

34. Miller RF, Fagerson MH, Staff NP, Wolfe R, Doerr T, Gottesman J, et al. Structure and functional connections of presynaptic terminals in the vertebrate retina revealed by activity-dependent dyes and confocal microscopy. J Comp Neurol. 2001;437: 129–55.

35. Haverkamp S, Grünert U, Wässle H, Grunert U, Wassle H. The cone pedicle, a complex synapse in the retina. Neuron. 2000;27: 85–95. doi:10.1016/S0896-6273(00)00011-8

36. Kolb H. The connections between horizontal cells and photoreceptors in the retina of the cat: Electron microscopy of Golgi preparations. J Comp Neurol. 1974;155: 1–14. doi:10.1002/cne.901550102

37. Schubert T, Weiler R, Feigenspan A. Intracellular Calcium Is Regulated by Different Pathways in Horizontal Cells of the Mouse Retina Intracellular Calcium Is Regulated by Different Pathways in Horizontal Cells of the Mouse Retina. J Neurophysiol. 2006;96: 1278–1292. doi:10.1152/jn.00191.2006

38. Lv T, Gong H-Q, Liang P-J. Caffeine-induced Ca2+ oscillations in type I horizontal cells of

721 the carp retina and the contribution of the store-operated Ca2+ entry pathway. PLoS
722 One. 2014;9: e100095. doi:10.1371/journal.pone.0100095

723 39. Feigenspan A, Babai N. Functional properties of spontaneous excitatory currents and
724 encoding of light/dark transitions in horizontal cells of the mouse retina. Eur J Neurosci.
725 2015;42: 2615–2632. doi:10.1111/ejn.13016

726 40. Hirano AA, Liu X, Boulter J, Grove J, Pérez de Sevilla Müller L, Barnes S, et al. Targeted
727 Deletion of Vesicular GABA Transporter from Retinal Horizontal Cells Eliminates Feedback
728 Modulation of Photoreceptor Calcium Channels. eNeuro. Society for Neuroscience;
729 2016;3: ENEURO.0148-15.2016. doi:10.1523/ENEURO.0148-15.2016

730 41. Ströh S, Sonntag S, Janssen-Bienhold U, Schultz K, Cimiotti K, Weiler R, et al. Cell-Specific
731 Cre Recombinase Expression Allows Selective Ablation of Glutamate Receptors from
732 Mouse Horizontal Cells. PLoS One. 2013;8: e83076. doi:10.1371/journal.pone.0083076

733 42. Rohlich P, van Veen T, Szel A. Two different visual pigments in one retinal cone cell.
734 Neuron. 1994;13: 1159–1166. doi:10.1016/0896-6273(94)90053-1

735 43. Baden T, Schubert T, Chang L, Wei T, Zaichuk M, Wissinger B, et al. A tale of two retinal
736 domains: Near-Optimal sampling of achromatic contrasts in natural scenes through
737 asymmetric photoreceptor distribution. Neuron. Elsevier Inc.; 2013;80: 1206–1217.
738 doi:10.1016/j.neuron.2013.09.030

739 44. Baden T, Berens P, Franke K, Román Rosón M, Bethge M, Euler T. The functional diversity
740 of retinal ganglion cells in the mouse. Nature. Nature Publishing Group; 2016;529: 345–
741 50. doi:10.1038/nature16468

742 45. Hendel T, Mank M, Schnell B, Griesbeck O, Borst A, Reiff DF. Fluorescence changes of
743 genetic calcium indicators and OGB-1 correlated with neural activity and calcium in vivo
744 and in vitro. J Neurosci. 2008;28: 7399–7411. doi:10.1523/JNEUROSCI.1038-08.2008

745 46. Tian L, Hires SA, Mao T, Huber D, Chiappe ME, Chalasani SH, et al. Imaging neural activity
746 in worms, flies and mice with improved GCaMP calcium indicators. Nat Methods. Nature

747 Publishing Group; 2009;6: 875–881. doi:10.1038/nmeth.1398

748 47. Franke K, Berens P, Schubert T, Bethge M, Euler T, Baden T. Balanced excitation and
749 inhibition decorrelates visual feature representation in the mammalian inner retina.
750 bioRxiv. 2016; 40642. doi:10.1101/040642

751 48. Sinha R, Hoon M, Baudin J, Okawa H, Wong ROL, Rieke F. Cellular and Circuit Mechanisms
752 Shaping the Perceptual Properties of the Primate Fovea. Cell. Elsevier; 2017;168: 413–
753 426.e12. doi:10.1016/j.cell.2017.01.005

754 49. Schubert T, Huckfeldt RM, Parker E, Campbell JE, Wong RO. Assembly of the outer retina
755 in the absence of GABA synthesis in horizontal cells. Neural Dev. 2010;5: 15.
756 doi:10.1186/1749-8104-5-15

757 50. Ueda Y, Kaneko A, Kaneda M. Voltage-dependent ionic currents in solitary horizontal cells
758 isolated from cat retina. J Neurophysiol. 1992;68: 1143–50.

759 51. Habermann CJ, O'Brien BJ, Wassle H, Protti DA, Wässle H, Protti DA. AII amacrine cells
760 express L-type calcium channels at their output synapses. J Neurosci. 2003;23: 6904–
761 6913.

762 52. Veruki ML, Oltedal L, Hartveit E. Electrical synapses between AII amacrine cells: dynamic
763 range and functional consequences of variation in junctional conductance. J
764 Neurophysiol. 2008/10/17. 2008;100: 3305–3322. doi:10.1152/jn.90957.2008

765 53. Shelley J, Dedek K, Schubert T, Feigenspan A, Schultz K, Hombach S, et al. Horizontal cell
766 receptive fields are reduced in connexin57-deficient mice. Eur J Neurosci. 2006;23: 3176–
767 3186. doi:10.1111/j.1460-9568.2006.04848.x

768 54. Grimes WN, Li W, Chávez AE, Diamond JS. BK channels modulate pre- and postsynaptic
769 signaling at reciprocal synapses in retina. Nat Neurosci. 2009;12: 585–592.
770 doi:10.1038/nn.2302

771 55. Liu X, Grove JCR, Hirano AA, Brecha NC, Barnes S. Dopamine D1 receptor modulation of
772 calcium channel currents in horizontal cells of mouse retina. J Neurophysiol. 2016;15573:

773 jn.00990.2015. doi:10.1152/jn.00990.2015

774 56. Sun X, Hirano AA, Brecha NC, Barnes S. Calcium-activated BK $_{Ca}$ channels govern dynamic
775 membrane depolarizations of horizontal cells in rodent retina. J Physiol. 2017; 1–39.
776 doi:10.1113/JP274132

777 57. Menger N, Wässle H. Morphological and physiological properties of the A17 amacrine cell
778 of the rat retina. Vis Neurosci. 2000;17: 769–780.

779 58. Haverkamp S, Grünert U, Wässle H. The cone pedicle, a complex synapse in the retina.
780 Neuron. 2000;27: 85–95. doi:10.1016/S0896-6273(00)00011-8

781 59. Behrens C, Schubert T, Haverkamp S, Euler T, Berens P. Connectivity map of bipolar cells
782 and photoreceptors in the mouse retina. bioRxiv. 2016; 65722. doi:10.1101/065722

783 60. Packer OS, Verweij J, Li PH, Schnapf JL, Dacey DM. Blue-Yellow Opponency in Primate S
784 Cone Photoreceptors. J Neurosci. 2010;30: 568–572. doi:10.1523/JNEUROSCI.4738-
785 09.2010

786 61. Mills SL, Tian L-M, Hoshi H, Whitaker CM, Massey SC. Three Distinct Blue-Green Color
787 Pathways in a Mammalian Retina. J Neurosci. 2014;34: 1760–1768.
788 doi:10.1523/JNEUROSCI.3901-13.2014

789 62. Breuninger T, Puller C, Haverkamp S, Euler T. Chromatic bipolar cell pathways in the
790 mouse retina. J Neurosci. 2011/04/29. 2011;31: 6504–6517. doi:31/17/6504
791 [pii]10.1523/JNEUROSCI.0616-11.2011

792 63. Borst A, Theunissen FE. Information theory and neural coding. Nat Neurosci. 1999;2: 947–
793 57. doi:10.1038/14731

794 64. Attneave F. Some informational aspects of visual perception. Psychol Rev. 1954;61: 183–
795 193. doi:10.1037/h0054663

796 65. Barlow H. Possible principles underlying the transformations of sensory messages. Sens
797 Commun. 1961;6: 57–58. doi:10.7551/mitpress/9780262518420.003.0013

66. Atick JJ. Could information theory provide an ecological theory of sensory processing? Netw Comput Neural Syst. 1992;3: 213–251. doi:10.1088/0954-898X_3_2_009

67. Storace DA, Braubach OR, Jin L, Cohen LB, Sung U. Monitoring brain activity with protein voltage and calcium sensors. Sci Rep. Nature Publishing Group; 2015;5: 10212. doi:10.1038/srep10212

68. Han Z, Jin L, Chen F, Loturco JJ, Cohen LB, Bondar A, et al. Mechanistic studies of the genetically encoded fluorescent protein voltage probe ArcLight. PLoS One. 2014;9: 1–21. doi:10.1371/journal.pone.0113873

69. Mank M, Reiff DF, Heim N, Friedrich MW, Borst A, Griesbeck O, et al. A FRET-based calcium biosensor with fast signal kinetics and high fluorescence change. Biophys J. Elsevier; 2006;90: 1790–6. doi:10.1529/biophysj.105.073536

70. Deniz S, Wersinger E, Schwab Y, Mura C, Erdelyi F, Szabó G, et al. Mammalian retinal horizontal cells are unconventional GABAergic neurons. J Neurochem. 2011;116: 350–362. doi:10.1111/j.1471-4159.2010.07114.x

71. Werblin FS. Transmission along and between rods in the Tiger Salamander Retina. J Physiol. 1978;280: 449–470.

72. Denk W, Strickler JH, Webb WW, Series N, Apr N. Two-Photon Laser Scanning Fluorescence Microscopy. Science (80-). 1990;248: 73–76. doi:10.1126/science.2321027

73. Chang L, Breuninger T, Euler T. Chromatic Coding from Cone-type Unselective Circuits in the Mouse Retina. Neuron. Elsevier Inc.; 2013;77: 559–571. doi:10.1016/j.neuron.2012.12.012

74. Dorostkar MM, Dreosti E, Odermatt B, Lagnado L. Computational processing of optical measurements of neuronal and synaptic activity in networks. J Neurosci Methods. Elsevier B.V.; 2010;188: 141–150. doi:10.1016/j.jneumeth.2010.01.033

75. Feigenspan A, Weiler R. Electrophysiological properties of mouse horizontal cell GABAA receptors. J Neurophysiol. 2004;92: 2789–2801. doi:10.1152/jn.00284.2004

824 76. Li B, McKernan K, Shen W. Spatial and temporal distribution patterns of Na-K-2Cl
825 cotransporter in adult and developing mouse retinas. Vis Neurosci. Cambridge University
826 Press; 2008;25: 109–23. doi:10.1017/S0952523808080164

827 77. Vardi N, Zhang LL, Payne J a, Sterling P. Evidence that different cation chloride
828 cotransporters in retinal neurons allow opposite responses to GABA. J Neurosci. 2000;20:
829 7657–7663. doi:20/20/7657 [pii]

830

831 # Figures

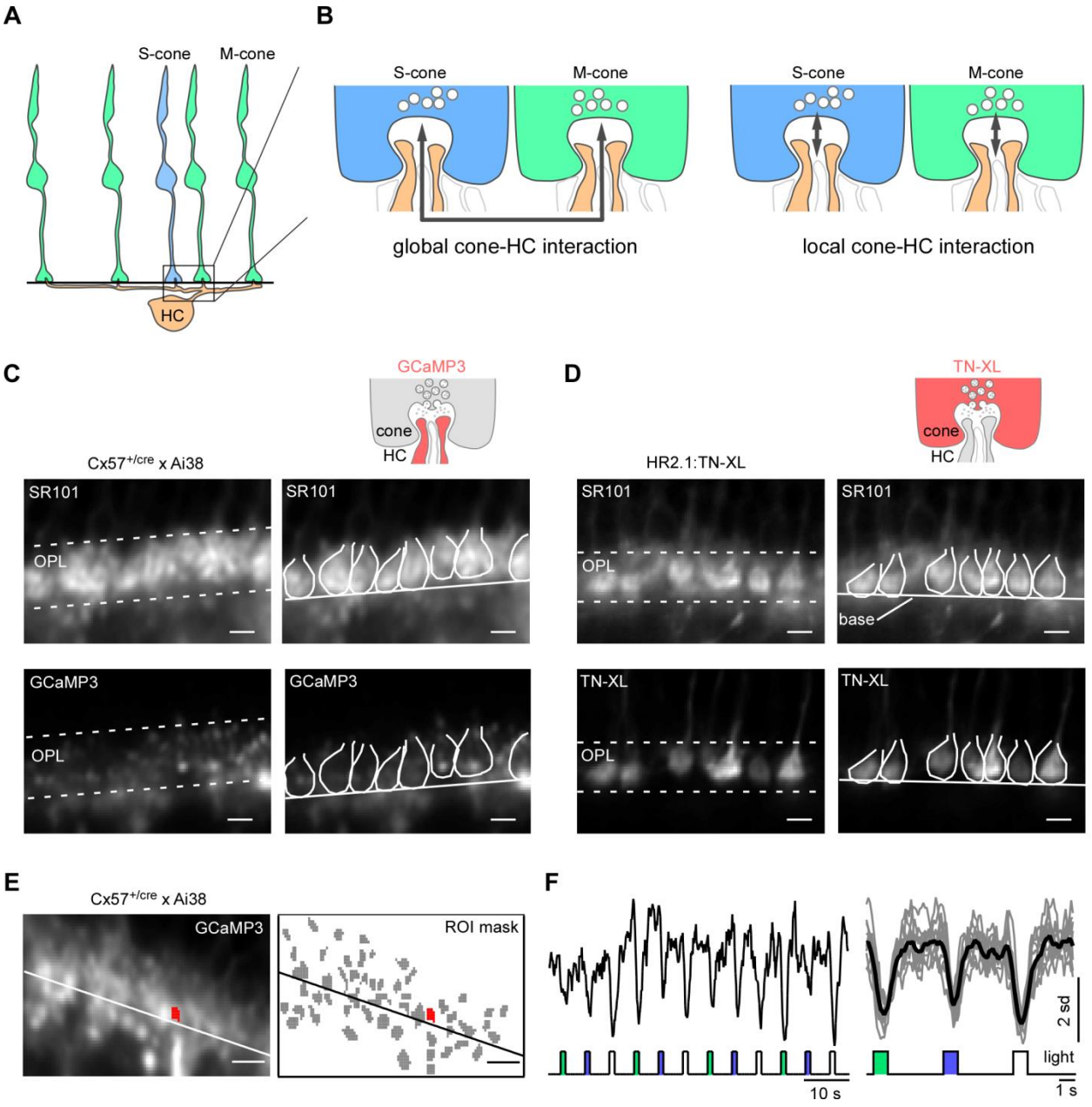

832

833 **Figure 1. Identification of cone axon terminals and HC processes in mouse retinal slices**

834 **A**. Schematic representation of the connectivity between S- (blue) or M-cones (green) and a
835 horizontal cell (HC, orange). The box corresponds to the enlarged schemata shown in B. The
836 black line indicates the cone axon terminal base (as shown in C-E). **B.** Neighbouring S- (blue) and

837 M-cones (green) with postsynaptic HC dendrites (orange). Bipolar cell dendrites are shown in
838 white. The arrows indicate the hypothesized spread of signals in HC dendrites. *Left:* Global
839 (lateral) signal spread along HC dendrites. *Right:* Local signal processing in HC dendritic tips. **C,D.**
840 Bath application of sulforhodamine 101 (SR101) (top images in C,D) to identify cone axon
841 terminals in retinal slices of the $Cx57^{+/cre}$ x Ai38 (C) and HR2.1:TN-XL mouse lines (D). Outlines of
842 cone axon terminals were manually drawn for illustration purposes; solid lines indicate cone
843 axon terminal base; dotted lines indicate outer plexiform layer (OPL) borders. Upper right
844 diagram depicts imaged synaptic compartment and biosensor used (red). **E.** *left*: GCaMP3-
845 labeled HC processes, with line marking cone axon terminal base (analogous to A, C and D).
846 *Right*: Regions of interest (ROIs; grey, exemplary ROI marked red) on HC processes were
847 automatically determined (Methods). **F**. Ca^{2+} responses to green, UV and "white" (GUW) 1-s
848 light flashes of exemplary ROI (in E); continuous Ca^{2+} trace (left) and average of n=10 trials for
849 each stimulus condition (right) are shown (Ca^{2+} signals de-trended by high-pass filtering at ~0.1
850 Hz and z-normalized, Methods). Scale bars, 5 µm.

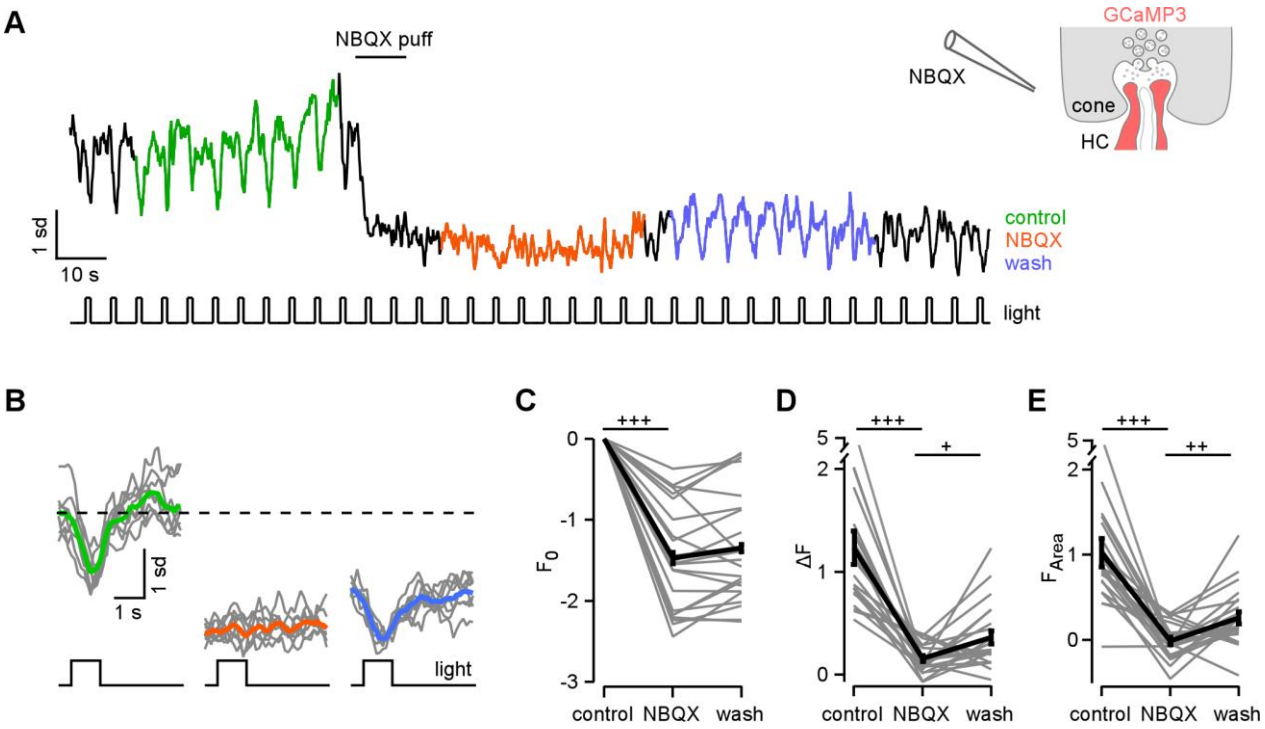

Figure 2. Light-evoked Ca^{2+} responses in HC processes are mediated by activation of AMPA/kainate-type glutamate receptors

A. Exemplary Ca^{2+} response of a HC process to white flashes before (control), after a puff of NBQX and during wash-out. **B.** Averaged responses for control (green), NBQX (orange) and wash (blue) (individual trials in grey). **C-E.** Quantification of NBQX effects on response baseline (F_0, C), amplitude (ΔF, D), and area-under-the-curve (F_{Area}, E) (average of n=23 ROIs from 4 slices, 2 animals). Error bars indicate SEM. +, $p \leq 0.025$; ++, $p \leq 0.005$; +++, $p \leq 0.0005$ (Bonferroni corrected significance threshold).

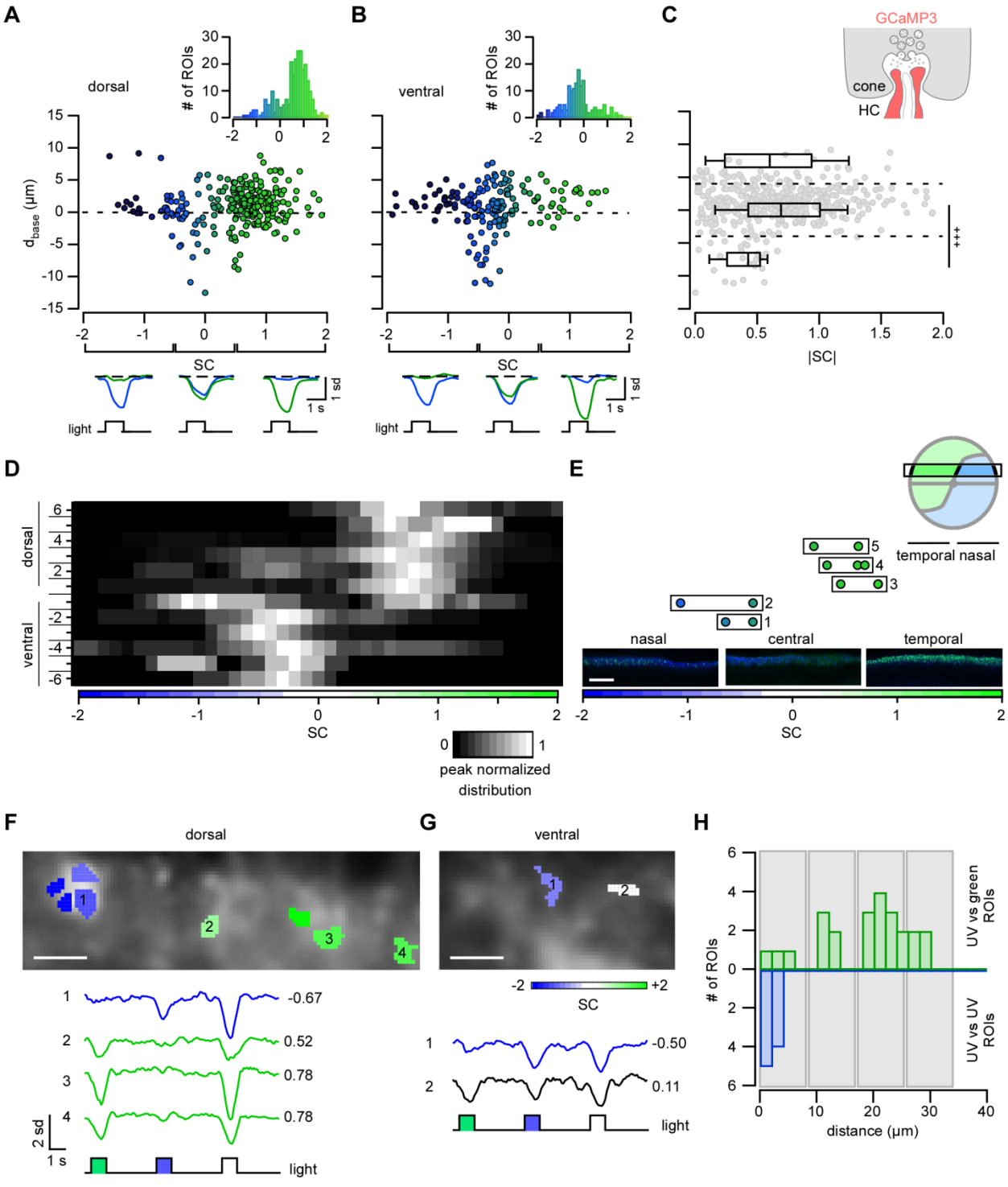

Figure 3. Light-evoked Ca^{2+} signals in HC dendrites reflect the dorso-ventral cone opsin expression gradient and local cone input

A,B. Plots showing distance between ROI and cone axon terminal base (d_{base}) as a function of spectral contrast (*SC*, see Methods) for dorsal (n=262 ROIs) (A) and ventral retina (n=161) (B). Insets show respective histograms of *SC* distributions. Below: Averaged Ca^{2+} signals in response to green and UV light flashes for different *SC* intervals (averages of n=10 trials). **C.** ROI distance to d_{base} as a function of $|SC|$ (ROIs from both dorsal and ventral retina). ROIs were separated into three groups (indicated by dashed lines) depending on d_{base}: above ($d_{base} > 4$ µm), below ($d_{base} < -4$ µm), and near the cone axon terminal base ($-4 \leq d_{base} \leq 4$ µm). **D.** *SC* distribution sorted by retinal slice position (from dorsal to ventral; distributions peak normalized for every slice position). **E.** *SC* of ROIs from 5 different locations on the same slice (boxes 1-5) cut along the naso-temporal axis (position +3, see D) and corresponding S- (blue) and M-opsin (green) immunolabeling in the temporal, central and nasal region. **F,G.** Examples of recording fields that contain ROIs with different *SC* for dorsal (F) and ventral (G) retina, with respective Ca^{2+} signals shown below (averages of n=10 trials). Colours reflect *SC* preference of each ROI (see colour bar in G). **H.** Spatial distribution of UV- (top histogram) and green- (bottom histogram) preferring ROIs relative to each UV ROI (at 0 µm) (for ROIs with $|SC| > 0.3$; n=22 ROIs from 7 fields, 3 dorsal and 2 ventral retinas). Grey boxes illustrate expected location of neighbouring cone axon terminals. +++, $p \leq 0.0005$ (Bonferroni corrected significance threshold). Scale bars, 200 µm in E, 5 µm in F, G.

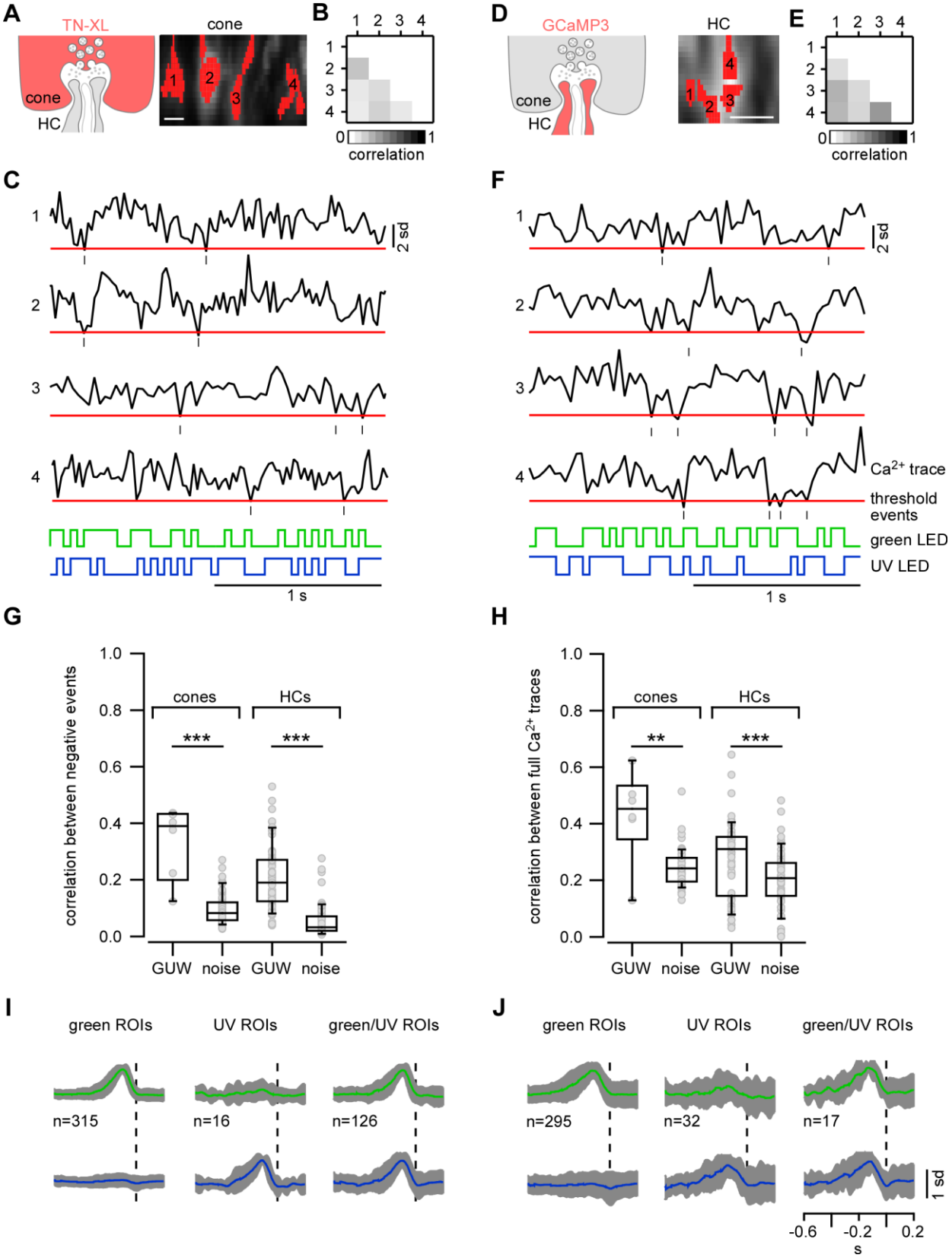

881

Figure 4. In the dorsal retina, light-evoked Ca^{2+} signals in neighbouring cone axon terminals and neighbouring HC dendrites show similar degrees of decorrelation

A-F. Exemplary neighbouring cone axon terminals in the HR2.1:TN-XL retina (A) and HC dendritic processes in the $Cx57^{+/cre}$ x Ai38 retina (D) with respective Ca^{2+} signals (C, F) in response to full-field 25-Hz coloured noise (Methods) with threshold (red line) used to detect (negative) events. Correlation of negative events for exemplary cones and HCs are shown in B and E. **G,H.** Average correlation per field for negative events only (G) and full Ca^{2+} traces (H) for cones and HCs in response to green, UV and white flashes (GUW) (cones: n=6 fields; HCs: n=60 fields) and to coloured noise (cones: n=65 fields; HCs: n=57 fields). **I,J.** Normalized time kernels of green ROIs (amplitude green kernel > 2 s.d. noise, left), UV ROIs (amplitude UV kernel > 2 s.d. noise; middle) and mixed ROIs (amplitude green and UV kernel > 2 s.d. noise; right) for cones (I) and HCs (J) (with 2 s.d. in grey). **, $p \leq 0.01$; ***, $p \leq 0.001$. Scale bars, 5 µm.

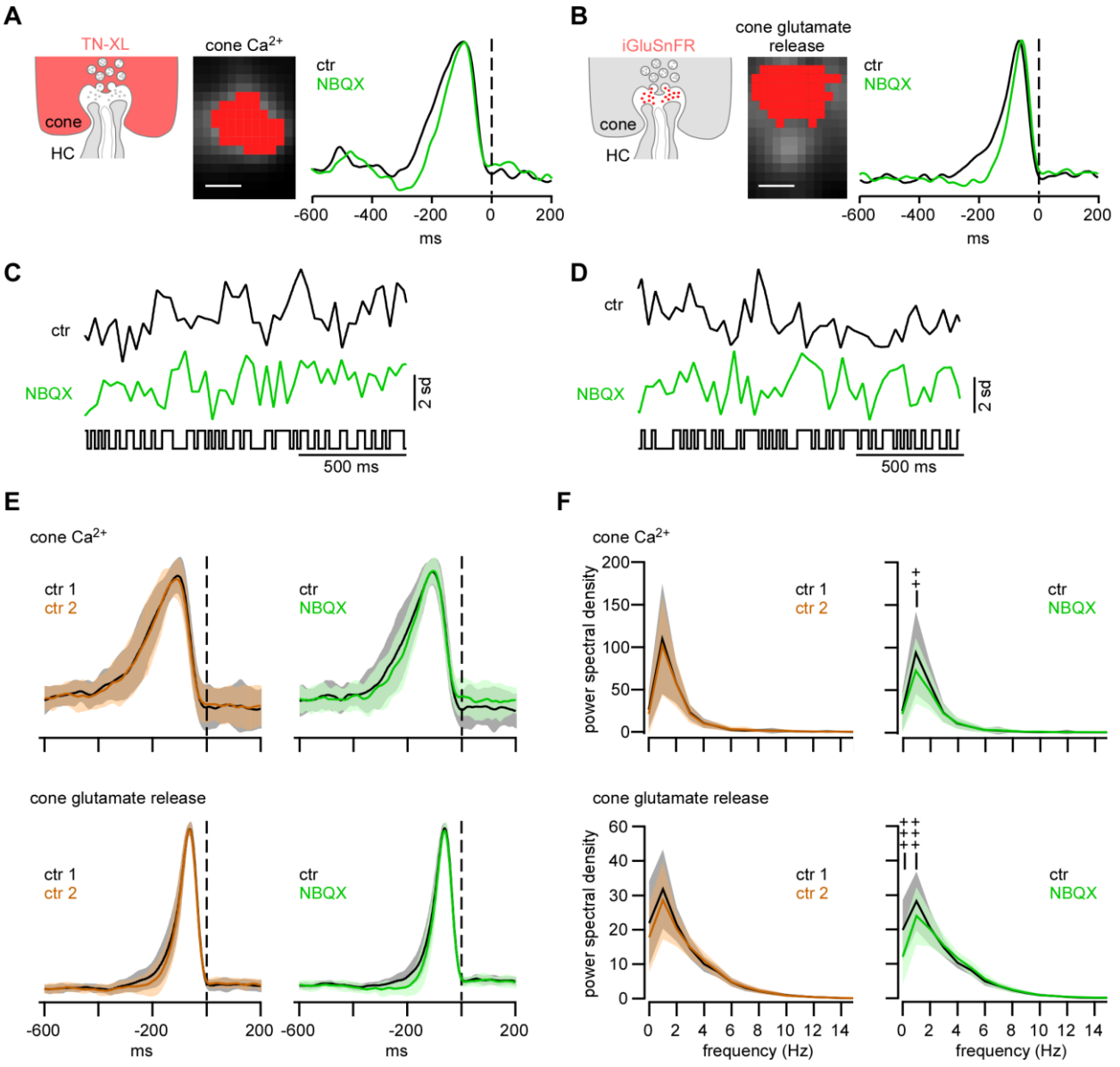

Figure 5. Local HC feedback modulates temporal properties of cone response

A-D. Exemplary ROIs of cone axon terminals, defined by TN-XL expression (A) or by iGluSnFR activity (B, Methods), with respective temporal receptive field kernels calculated from response to a full-field 60-Hz binary noise stimulus (raw traces in C, D; Methods) for control condition (black traces in A-D) and during bath application of NBQX (green traces in A-D). **E.** Normalized time kernels for cone Ca^{2+} (upper panel) and glutamate release (lower panel) for control

condition (ctr1, ctr2; left) and with NBQX (right) (cone Ca^{2+}: ctr, n=61 ROIs; NBQX, n=48 ROIs; cone glutamate release: ctr, n=76 ROIs; NBQX, n=47 ROIs; shaded areas indicate 1 s.d). **F.** Periodograms (Methods) generated from cone kernels (E) using a discrete Fourier transform: cone Ca^{2+} (upper panel) and glutamate release (lower panel) for control condition (left) and with NBQX (right) (shaded areas indicate 1 s.d.). ++, $p \leq 6.66 \cdot 10^{-4}$; +++, $p \leq 6.66 \cdot 10^{-5}$ (Bonferroni corrected significance threshold). Scale bars, 2.5 µm.

Tables

Table 1. Pharmacology for AMPA/KA-type glutamate receptors

	number of mice/slices/ROIs	control	drug	wash
NBQX puff application				
F_0 [s.d.]	2/4/23	0	-1.470 ± 0.069 ($p=2.384\cdot10^{-7}$ +++)	-1.348 ± 0.046 (p=0.033)
ΔF [s.d.]		1.235 ± 0.163	0.156 ± 0.029 ($p=2.384\cdot10^{-7}$ +++)	0.362 ± 0.064 (p=0.007 +)
F_{Area} [a.u.]		1.024 ± 0.167	-0.012 ± 0.044 ($p=4.768\cdot10^{-7}$ +++)	0.257 ± 0.071 (p=0.003 ++)

NBQX, AMPA/KA-type glutamate receptor antagonist; Ca^{2+} baseline (F_0), amplitude (ΔF) and area-under-the-curve (F_{Area}) of light-evoked Ca^{2+} responses.

912 **Table 2. Pharmacology to block voltage-gated Ca^{2+} channels and Ca^{2+} release from stores**

	number of mice/slices/ROIs	AMPA/KA puff 1 ΔF_1 [s.d.]	AMPA/KA puff 2 ΔF_2 [s.d.] (ΔF_2 vs. ΔF_1)	$\Delta F_2/\Delta F_1$ (vs. control)
control	2/2/23	3.106±0.286	1.648 ± 0.198 ($p=1.025\cdot10^{-5}$ ***)	0.564 ± 0.062
verapamil	2/3/18	2.011±0.177	0.426 ± 0.130 ($p=7.629\cdot10^{-6}$ ***)	0.230 ± 0.052 ($p=9.088\cdot10^{-5}$ +++)
thapsigargin	3/5/13	1.445±0.126	0.494±0.154 (p=0.0002***)	0.340 ± 0.082 (p=0.049)

913

914 verapamil, L-type VGCC blocker; thapsigargin, inhibitor of sarco-endoplasmic reticulum Ca^{2+}-

915 ATPases; amplitude puff 1 (ΔF_1), amplitude puff 2 (ΔF_2), ratio puff 2/puff 1 ($\Delta F_2/\Delta F_1$)

Supplementary Material

$GABA_A$ receptor activation modulates the intracellular Ca^{2+} level in distal HC tips

Horizontal cells are GABAergic [17] but the role of GABA for the HC feedback to cones is still controversial [24]. In mouse, cones do not express ionotropic GABA receptors [16], while HCs do [75]. Therefore, it has been proposed that GABA release from HCs activates $GABA_A$ auto-receptors and thereby modulates ephaptic and pH-mediated feedback to cones [17,19].

To test if GABA auto-reception affects Ca^{2+} signals in HC processes we puff-applied the $GABA_A$ receptor agonist muscimol while presenting light flashes (Suppl. Fig. 3A,B). Despite some variability, muscimol caused on average a small but significant increase in F_0 (by 0.32 ± 0.13 s.d., p=0.011 for muscimol vs. control; n=20 ROIs from 4 slices, 2 mice; Suppl. Fig. 3C and Suppl. Table 1) which was reversible (0.03 ± 0.15 s.d., p=0.007 for muscimol vs. wash-out). The size of the light responses did not change significantly (Suppl. Fig. 3D,E, Suppl. Table 1). That Ca^{2+} levels increase upon $GABA_A$ (auto-)receptor activation is consistent with earlier reports that suggested high intracellular Cl^- levels in HC dendritic tips due to the expression of $Na^+/K^+/Cl^-$ co-transporters [76,77]. Thus, it is likely that $GABA_A$ receptor activation caused a Cl^- efflux, with the resulting depolarisation activating voltage-gated Ca^{2+} channels (VGCCs). We also puff-applied the $GABA_A$ receptor antagonist gabazine but we did not find any consistent effects (n=33 ROIs from 4 slices, 2 mice; Suppl. Fig. 3F-J, Suppl. Table 1), in line with results for mouse cone axon terminals (for discussion, see [16]). Our data provide evidence that GABA auto-reception plays a role in modulating the activity in distal HC processes and, thus, in shaping cone output [17,40].

Contrast encoding in the dendritic tips of HCs

Mouse cones differ in their encoding of achromatic contrast depending on their location on the retina [43]: dorsal M-cones respond equally well to bright and dark flashes (positive and negative contrasts, respectively), whereas ventral S-cones prefer dark over bright contrasts. We tested if this contrast coding is preserved in HC dendrites (Suppl. Fig. 5) by presenting bright and dark flashes of different "colours" (Suppl. Fig. 5A-C, see "contrast and colour" protocol in Methods) and calculating for each ROI the spectral contrast (*SC*) preference and its preference for dark over bright contrasts ("dark-light index", *DLi*, Methods). The majority of HC ROIs generally responded preferentially to dark over bright stimuli (green: $\Delta F_{dark} = 1.44 \pm 0.60$ vs. $\Delta F_{bright} = 0.62 \pm 0.46$, $p=8.389 \cdot 10^{-9}$, n=57; UV: $\Delta F_{dark} = 1.63 \pm 0.56$ vs. $\Delta F_{bright} = 0.55 \pm 0.35$, $p=2.288 \cdot 10^{-25}$, n=99) (Suppl. Fig. 5A-D). Nevertheless, the *DLi* distribution for dorsal ROIs was broader than that for ventral ROIs and shifted towards zero (means: -0.51 vs -0.70, p = 0.0093, t-test; variance: 0.22 vs. 0.06, p=0.000004, Bartletts test; Suppl. Fig. 5E). In general, the *DLi* was independent on *SC* (Suppl. Fig. 5F) and F_0 (Suppl. Fig. 5G). Overall, the contrast preference in HC processes shows a trend along the dorso-ventral retina axis that is reminiscent of what was earlier shown for cones [43], arguing that distal HC dendrites inherit properties of local cones.

Supplementary Figures

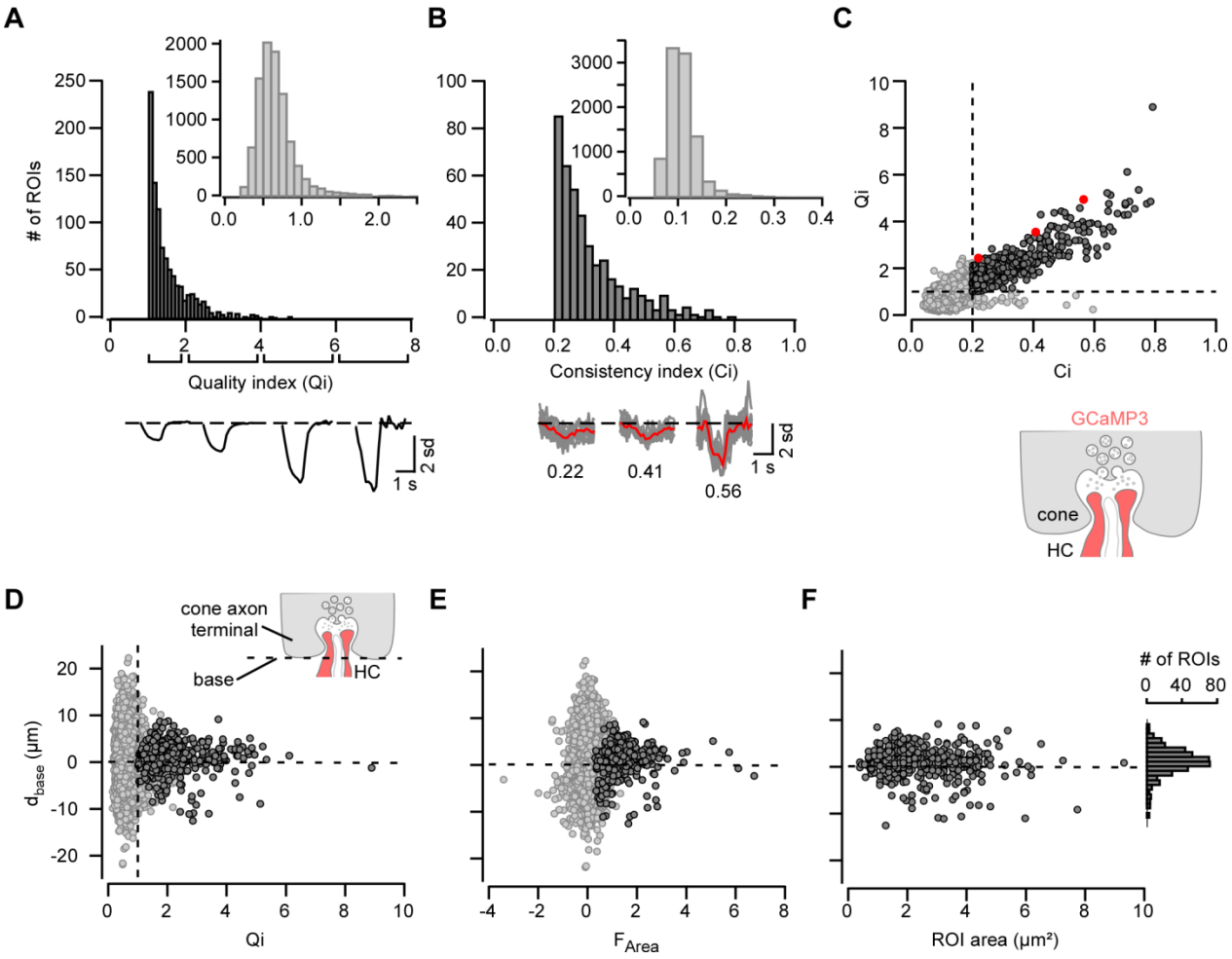

Supplementary Figure 1. Selection of ROIs on horizontal cell processes based on their light-evoked Ca^{2+} signals

A. Distribution of quality index (*Qi*), defined as ratio between Ca^{2+} response amplitude to white flash and s.d. of noise (Methods). Only ROIs with $Qi \geq 1$ (dark grey) were considered for further analysis (inset shows distribution of discarded ROIs). *Below*: Average Ca^{2+} responses across ROIs for different *Qi* intervals. **B.** Distribution of consistency index (*Ci*), defined as ratio between variance of the mean and mean of variance (Methods). Only ROIs with $Ci \geq 0.2$ (dark grey) were

961 considered for further analysis (inset shows distribution of discarded ROIs). *Below*: Exemplary
962 Ca^{2+} traces for different *Ci* values (mean in red, n=10 trials in grey). **C.** *Qi* as a function of *Ci*, with
963 ROIs passing both criteria shown as dark-grey dots (n=423 of 9,912 ROIs passed both criteria).
964 Red dots indicate ROIs of example traces in B. **D,F.** Distance of ROI (centre of mass) to cone axon
965 terminal base (d_{base}) as a function of *Qi* (D, the dashed line indicates the cone base), area-under-
966 the-curve (F_{Area}, E) and ROI area (F). ROI areas (F) above the cone axon terminal base ($d_{base} > 0$;
967 2.45 ± 0.07 µm^2, n=292) and below ($d_{base} < 0$; 2.87 ± 0.30 µm^2, n=131) were not significantly
968 different (p=0.248). Histogram shows distribution of ROIs along the cone terminal base. Diagram
969 on the right depicts imaged synaptic compartment and used biosensor (red).

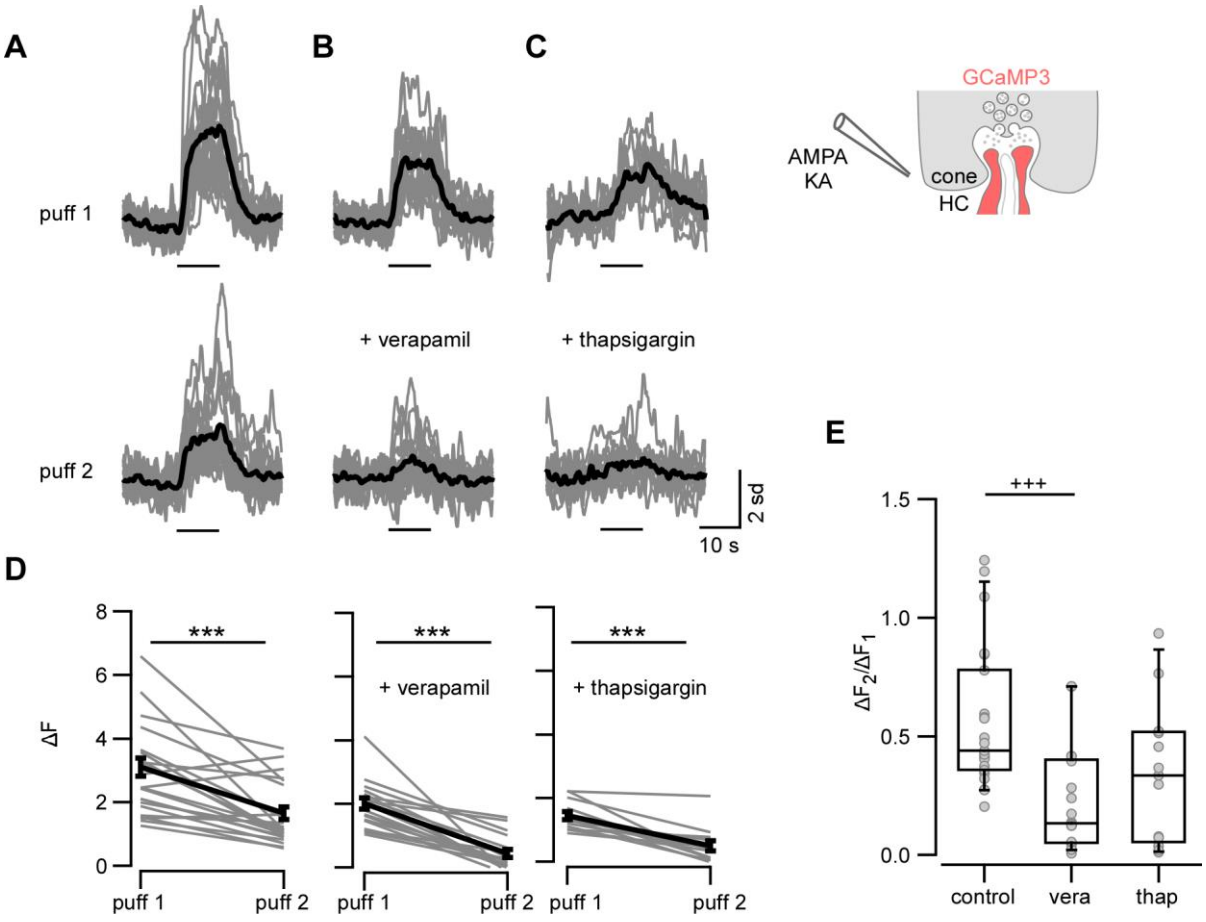

Supplementary Figure 2. Ca^{2+} signals in HC dendrites are mediated by voltage-gated Ca^{2+} channels and possibly intracellular Ca^{2+} stores.

A-C. Ca^{2+} signals in HC processes evoked by two consecutive AMPA/KA puffs (bars indicate puff timing). *Top row*: in standard bathing medium; *bottom row*: normal medium (A, n=23 ROIs from 2 slices, 2 mice), during bath application of verapamil (B, n=18, 3 slices, 2 mice) and thapsigargin (C, n=13, 5 slices, 3 mice). **D**. Quantification of drug effects on response amplitude ΔF (error bars indicate SEM; ***, $p \leq 0.001$) **E.** Ratios between ΔF_2 (2^{nd} puff) and ΔF_1 (1^{st} puff) control, verapamil (vera) and thapsigargin (thap) (+++, $p \leq 0.0005$) (Bonferroni corrected significance threshold).

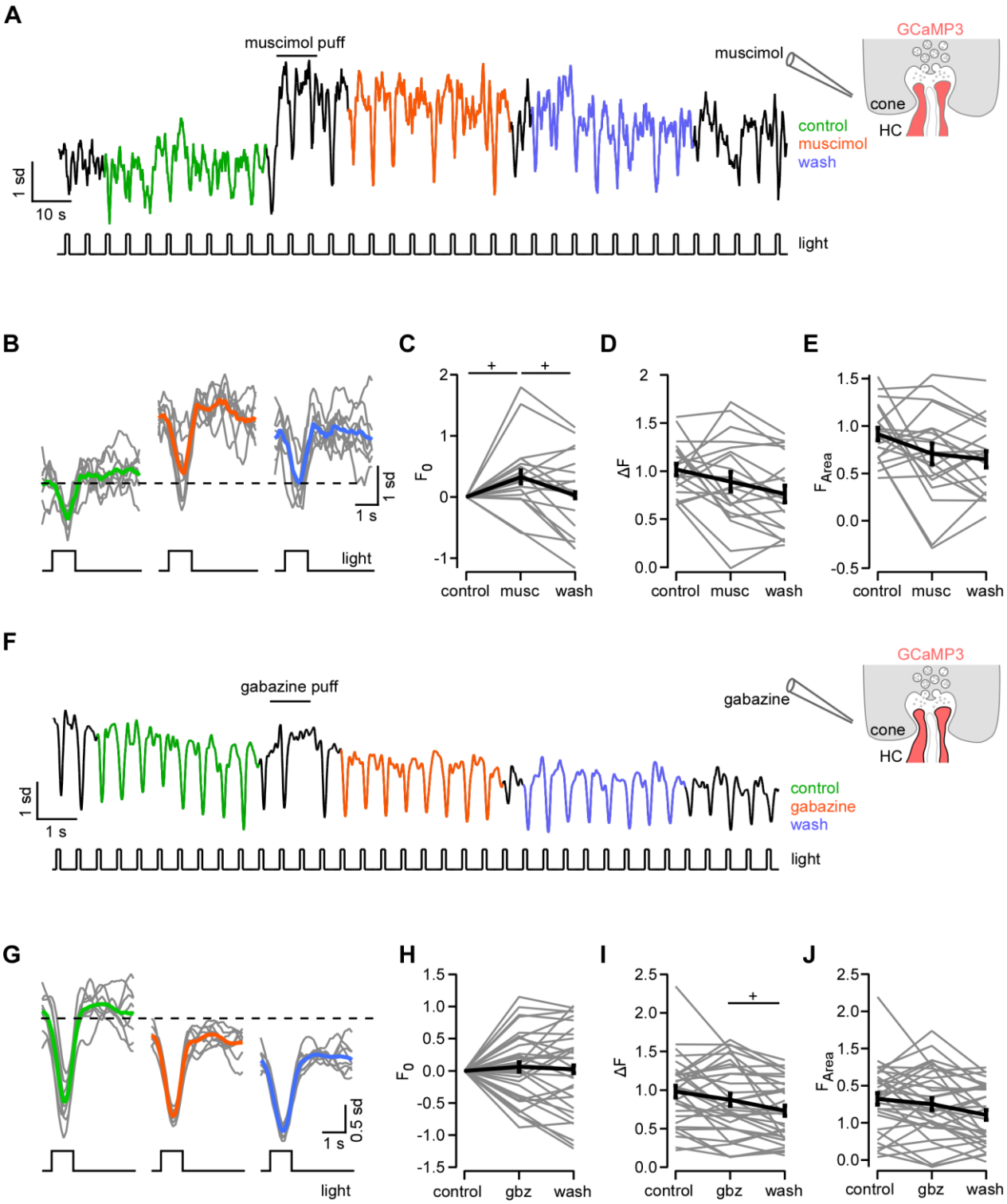

Supplementary Figure 3. GABA modulates light-evoked Ca^{2+} signals in HC dendrites

A. Exemplary Ca^{2+} response of a HC process to white flashes before (control), after a puff of the $GABA_A$ receptor agonist muscimol and during wash-out. **B.** Averaged responses for control (green), muscimol (orange) and wash-out (blue). **C-E** Quantification of muscimol (musc) effects on response baseline (F_0, C), amplitude (ΔF, D) and area-under-the-curve (F_{Area}, E) (average of n=20 ROIs from 4 slices, 2 mice). **F.** Experiment as in (A) but for the $GABA_A$ receptor antagonist gabazine. **G.** Averaged responses for control, gabazine and wash-out. **H-J.** Quantification of gabazine (gbz) effects (average of n=33 ROIs, 4 slices, 2 mice). Error bars indicate SEM. +, $p \leq 0.025$ (Bonferroni corrected significance threshold).

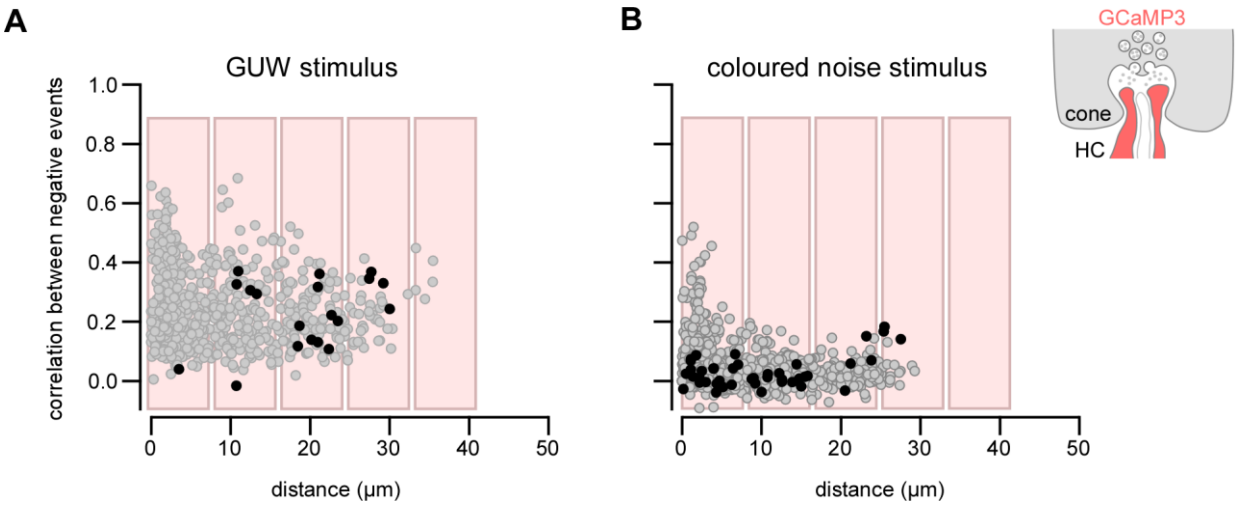

990

991 **Supplementary Figure 4. Correlation between negative events in HC processes**

992 **A,B.** Correlation between negative events in HC processes ($Cx57^{+/cre}$ x Ai38 mouse line) for all
993 combinations of ROIs present in the same field as a function of their distance; for GUW stimulus
994 (A) and coloured noise (B). Dark circles indicate the combinations between "purely" green and
995 "purely UV" ROIs (GUW, $|SC| > 0.4$; coloured noise, amplitude UV or green kernel > 2 s.d.
996 noise). Reddish boxes illustrate expected location of neighbouring cone axon terminals.

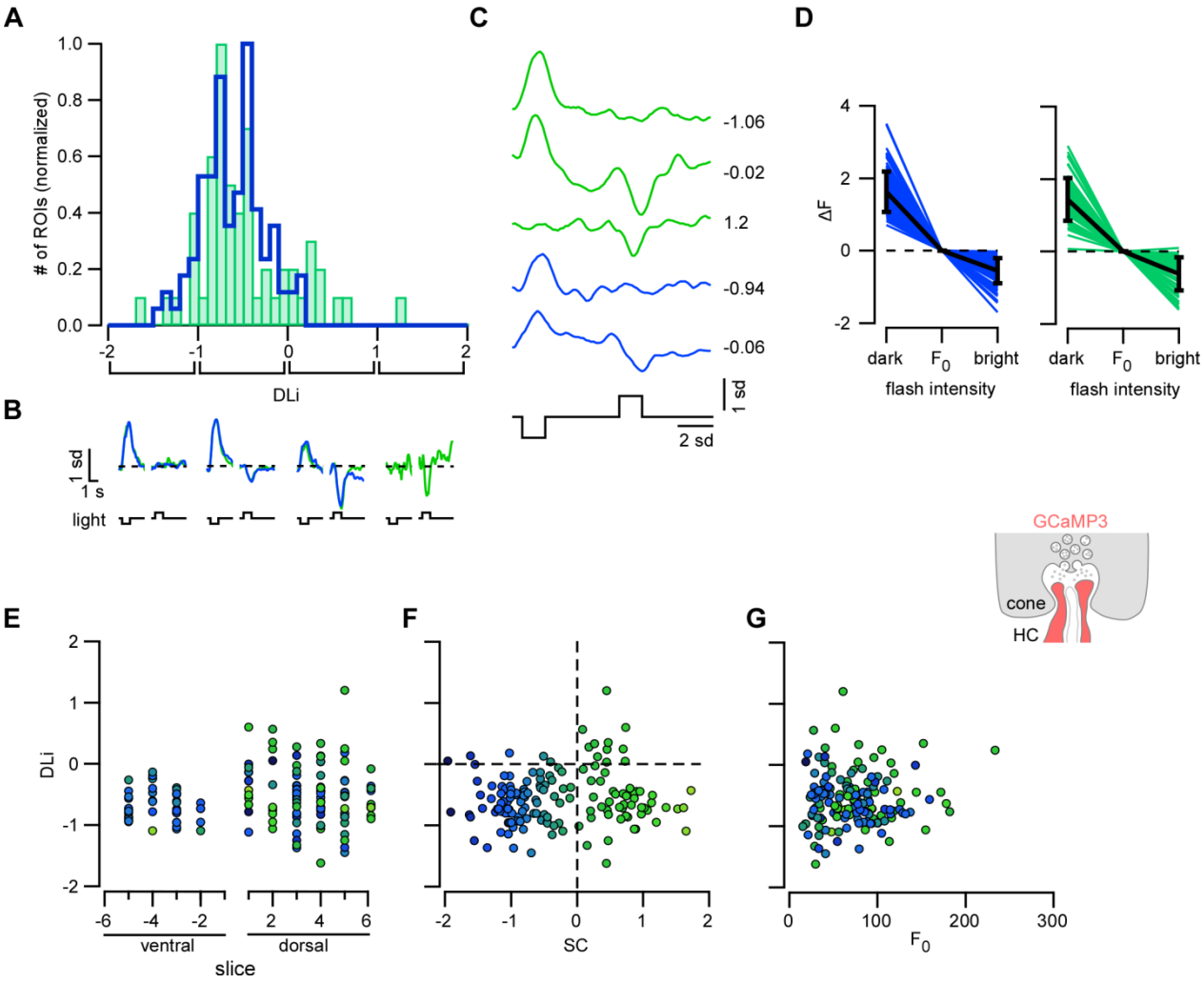

997

998 **Supplementary Figure 5. Contrast preference of Ca^{2+} responses in HC processes**

999 **A.** Histogram of dark-light index distribution (*DLi*; see Methods) for green (*SC*>0; n=57 ROIs) and

1000 UV (SC<0; n=99 ROIs). **B.** Averaged Ca^{2+} signal in response to green and UV, dark and bright

1001 flashes for different *DLi* intervals (averages of n=8 trials). **C.** Exemplary green and UV ROIs

1002 responding to dark and bright flashes (averages of n=8 trials). Values indicate *DLi*. **D.** Response

1003 amplitudes (*ΔF*) for UV (left) and green ROIs (right) to dark and bright flashes (F_0, baseline). **E-G.**

1004 *DLi* plotted as a function of slice position (E), *SC* (F) and baseline (F_0, G). Colours reflect *SC*

1005 preference of each ROI. **E.** Error bars indicate s.d.

Supplementary Tables

Supplemental Table 1. Pharmacology for $GABA_A$ auto-receptors on HCs

	Number of mice/slices/ROIs	control	drug	wash
muscimol puff application				
F_0 [s.d.]	2/4/20	0	0.323±0.126 (p=0.011 +)	0.029±0.149 (p=0.007 +)
ΔF [s.d.]		1.0166±0.061	0.891±0.102 (p=0.330)	0.762±0.087 (p=0.040)
F_{Area} [a.u.]		0.915±0.067	0.707±0.110 (p=0.154)	0.649±0.086 (p=0.452)
gabazine puff application				
F_0 [s.d.]	2/4/33	0	0.0622±0.076 (p=0.525)	0.024±0.060 (0.437)
ΔF [s.d.]		0.981±0.0762	0.874±0.0816 (0.126)	0.733±0.067 (p=0.009 +)
F_{Area} [a.u.]		0.822±0.079	0.751±0.081 (p=0.296)	0.606±0.0679 (p=0.027)

muscimol, $GABA_A$ receptor agonist; gabazine, $GABA_A$ receptor antagonist; Ca^{2+} baseline (F_0), amplitude (ΔF) and area-under-the-curve (F_{Area}) of light-evoked Ca^{2+} responses